Sina Ramoser, BSc

Fabrication and testing of organo-lead halide perovskite solar cells and lead-free perovskite solar cells

MASTER'S THESIS

to achieve the university degree of

Diplom-Ingenieurin

Master's degree programme: Technical Chemistry

submitted to

Graz University of Technology

Supervisor

Assoc. Prof. DI Dr. Gregor Trimmel

Institute for Chemistry and Technology of Materials

Graz, January 2015

AFFIDAVIT

I declare that I have authored this thesis independently, that I have not used other than the declared sources/resources, and that I have explicitly indicated all material which has been quoted either literally or by content from the sources used. The text document uploaded to TUGRAZonline is identical to the present master‘s thesis.

Date

Signature

ABSTRACT

Perovskite solar cells are a promising new organic inorganic photovoltaic technology, which achieved great improvements in the last few years. The perovskite consist of an organic cation such as methylammonium, a metal cation such as Pb^{2+} and an anion such as iodide.

In this work different architectures of perovskite solar cell were explored. First, the optimal conditions for lead perovskite solar cells made of solution method were examined based on literature recipes. In order to achieve this, the optimal fabrication conditions had to be identified. Thus, two different standard architectures were used.

In the first assembling the solar cells were built on compact and mesoporous TiO_x underlayers and a hole transport material (HTM) was coated on the perovskite active layer. The second architecture is an organic assembling where the active layer was sandwiched between poly(3,4-ethylenedioxythiophene) polystyrene sulfonate (PEDOT:PSS) and phenyl-C61-butyric acid methyl ester (PCBM). For the preparation of the active layer different manufacturing methods, manufacturing conditions, solvents and concentrations were tested. The active layer in the first architecture was either made from a solution of PbI_2 and methyl-ammonium-iodide (MAI) or it was prepared by dipping a PbI_2 coated substrate into a solution of MAI. The solvent and the concentration were dependent on the way the active layer was fabricated. For each method the annealing conditions were adapted and two different HTMs were tested. The efficiency of the best prepared perovskite solar cell was 8.62%. Furthermore, different lead halogenides were tested in the dipping and solution method.

Lead perovskite solar cells may harm the environment because they form PbI_2 when they are exposed to moisture. Thus, lead free alternatives are more interesting for commercial applications. In this master thesis two lead free alternatives were tested. The first one was a tin perovskite solar cell. The second opportunity for lead free solar cells which was tested was the BiI_3 solar cell. In both cases the conditions of manufacturing were optimized. Nevertheless, the best performing lead-free solar cell could only achieve an efficiency of 0.032%.

To determine the solar cell parameters current voltage curves were measured. The solar cells and layers were characterized using UV/Vis spectroscopy and an external quantum efficiency measurement of the lead solar cell was performed. In order to get a better insight in the actual structure of the solar cell, scanning electron microscopy (SEM) cross section images were taken. The crystal structure of the active layers was determined with x-ray diffraction (XRD) measurements.

ZUSAMMENFASSUNG

Perowskitsolarzellen sind eine neue vielversprechende organisch-anorganische Photovoltaiktechnologie, welche in den letzten Jahren immer bessere Effizienzen erzielten. Der Perowskit besteht aus einem organischen Kation, wie Methylammonium, einem Metallkation, wie Pb^{2+} und einem Anion, wie Iodid. In dieser Arbeit wurden verschiedene Architekturen von Perowskit-Solarzellen erforscht. Zuerst mussten die optimalen Bedingungen basierend auf Kenntnissen aus der Literatur für eine Blei-Perowskit-Solarzelle gefunden werden. Um das zu erzielen, mussten die optimalen Herstellungsbedingungen gefunden werden. Dafür wurden zwei verschieden Architekturen verwendet.

In der ersten Architektur wurden die Solarzellen auf eine kompakte und eine mesoporöse TiO_x-Schicht gebaut und auf die Aktivschicht wurde ein Lochtransportmaterial aufgetragen. Im zweiten Aufbau wurde die Perowskitschicht in einem organischen Aufbau zwischen Poly(3,4-ethylenedioxythiophene)-poly(styrenesulfonate) und [6,6]-Phenyl-C61Buttersäuremethylester verbaut. Für die Herstellung der Aktivschicht wurden verschiedene Herstellungsarten und -bedingungen, Lösungsmittel und Konzentrationen getestet. Die Aktivschicht kann aus der Lösung von PbI_2 und Methylammoniumiodid oder durch tauchen einer PbI_2-Schicht in eine Methylammoniumiodid-Lösung hergestellt werden. Das Lösungsmittel und die Konzentration hängen von der Art der Aktivschichtherstellung ab. Für jede Aktivschichtherstellungsart wurden die Temperbedingungen angepasst. Zwei verschiedene Lochtransportmaterialien wurden ausprobiert. Die Effizienz der besten hergestellten Perowskitsolarzelle war 8,62%. Außerdem wurden mehrere Bleihalogenide in beiden Aktivschichtherstellungsarten getestet. Blei-Perowskit-Solarzellen können die Umwelt schädigen weil beim Kontakt mit Wasser Bleiiodid entsteht. Darum sind bleifreie Alternativen interessanter für kommerzielle Anwendungen. In dieser Masterarbeit wurden zwei bleifreie Alternativen getestet. Die erste Möglichkeit war das Bleiperowskit durch Zinnperowskit zu ersetzen. Die zweite getestete Möglichkeit war BiI_3 als Aktivschicht in eine Solarzelle einzubringen. Für die neue Aktivschichten wurden wieder alle Herstellungsbedingungen angepasst. Trotzdem hatte die bestfunktionierende Bleifreie-Solarzelle nur eine Effizienz von 0,032%.

Die Solarzellenparameter wurden mittels einer Strom-Spannungsmessung ermittelt. Die Solarzellen und Schichten wurden mittels eines UV/Vis Spektrometers charakterisiert und die externe Quantenausbeute von Blei-Perowskit-Solarzellen wurde bestimmt. Um einen besseren Einblick in die verschiedenen Strukturen zu bekommen, wurden Bilder des Querschnitts mit einem Sekundärelektronenmikroskop aufgenommen. Die Kristallstruktur der Aktivschichten wurde mittels einer Röntgenbeugungsanalyse ermittelt.

ACKNOWLEDGEMENTS

First of all I want to thank Assoc. Prof. DI Dr. Gregor Trimmel for providing me with the opportunity to write this master thesis in his working group as well as for his pleasant and permanent support.

A very special thanks goes to Dr. Verena Harum for her inspiring guidance and friendly advice. She always had an open ear for questions and discussions. Moreover I want to thank Dr. Thomas Rath, who introduced me to this topic and always had time for a helping advice.

I am using this opportunity to express my gratitude to everyone who supported me during my master thesis, especially my working group. Another thanks goes to the people at the Institute for Chemistry and Technology of Materials (ICTM) and all my colleagues I have met during my studies.

Furthermore, I would like to thank Birgit Kunert and Prof. Roland Resel for the XRD measurements and I also want to express my gratitude to Dr. Angelika Reichmann for the SEM pictures.

A special thanks goes to my whole family, who supported and motivated me during the course of my studies and my deepest gratitude is dedicated to my parents because without them this would not be possible.

Table of contents

I INTRODUCTION

Energy is the driving force in scientific, economic and social progress in these times. The path we are currently on has to be changed otherwise energy related greenhouse-gas emissions will lead to catastrophic climate changes.[1]

Thus, the energy mix should consist of more renewable energy. In 2012 only 13% of the total primary energy supply came from sustainable sources, as shown in Figure 1. The total primary energy supply in 2012 was 13 371 million tonnes of oil equivalent (Mtoe)[2]. The present global energy supply is mainly based on fossil fuels which cause the climate change and the increasing CO_2 concentration in the atmosphere.

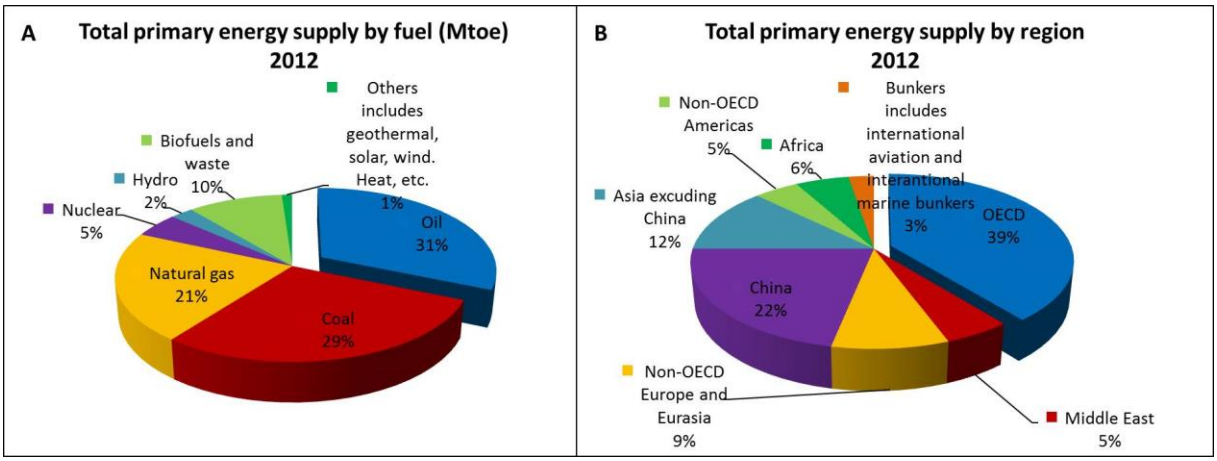

Figure 1 Total primary energy supply (data taken from © OECD/IEA 2013 World Energy Outlook, IEA Publishing. Licence: http://www.iea.org/t&c/termsandconditions/])[2]

The production of secure, clean, sustainable energy is one of the most important challenges in the 21st century. Solar energy is inexhaustible and CO_2-emission-free. The sun provides $1.4*10^5$ TW power to the earth every year and $3.6\ 10^4$ TW of this power is usable for us. The world's power consumption was 17 TW in 2012. Thus, the whole world could theoretically be powered with energy from the sun.

Photovoltaic is one of the best ways to use solar energy. A direct conversion of sunlight into electricity without any heat engine to interfere is possible with this technology. Many different photovoltaic technologies such as monocrystalline silicon solar cell, polycrystalline silicon solar cell, amorphous silicon solar cell, cadmium telluride solar cell, copper indium gallium selenide/sulphide solar cell and dye sensitized solar cell are available today. One of the most recent developments are perovskite solar cells.

1. Aim of this thesis

The subject of this work was the preparation and investigation of lead and lead-free perovskite solar cells. Perovskite solar cells are constructed with a thin layer of a material which crystallizes in a perovskite structure. First, a good-working organo-lead halide perovskite solar cell had to be built. For this, different preparation routes for the solar cells and various solvents and concentrations of the solution for the preparation of the perovskite layer are used.

Moreover, the perovskite is tested in two different assemblings. The first one is a heterojunction perovskite solar cell with TiO_x as an underlayer and a hole transport material on top. In this assembling two different preparation methods for the perovskite are tested. The second one is the perovskite/PCBM planar heterojunction solar cell with PEDOT:PSS as an underlayer and PCBM as a hole blocking material.

The performance of the solar cells is identified through a I/V characteristics. Furthermore, the solar cells are investigated with UV-Vis measurements, external quantum efficiency measurements and scanning electron microscopy. The lead perovskite layer is characterized with XRD measurements, optical band gap measurements and also UV-Vis measurements.

Lead and lead(II)iodide which could be formed when the solar cells come in contact with water are very toxic and harmful to the environment. The use of lead is also restricted in the restriction of hazardous substances directive (RoHS). [3] Thus, two lead-free alternatives are tested in solar cell application. The first one is an organo-tin halide perovskite. For the use of the tin perovskite in solar cells the conditions are adapted. These solar cells are also characterized with UV-Vis measurements and the optical band gap of the tin perovskite layer is determined.

The second alternative is BiI_3 which crystallizes in a perovskite similar structure. The conditions for the solar cells preparation are adapted for BiI_3. BiI_3 is used in two different assemblings, the heterojunction perovskite solar cell and the perovskite/PCBM planar heterojunction solar cell. The BiI_3 is characterized with XRD and UV-Vis measurements and the optical band gap is investigated.

II BASICS

1. History of solar cells

The development of photovoltaics begins as Alexandre-Edmond Becquerel in 1839 found out that shining light on a liquid electrolyte near an electrode produces an electrical current. This was the first documented link between light and electrical power. [4,5]

Willoughby Smith discovered the photoconductivity of selenium in 1873, so that the first solar cells made from selenium wafers were described by the American inventor Charles Fritts in 1883. In 1900 Max Planck postulated the formula for the spectrum of heat radiation. This formula provided the foundation for quantum solar energy conversion and photovoltaics. [4,5]

In the 1930s advances in semiconductor research were made. The understanding of semiconductor junction and their application in Schottky-barrier Cu_2O/Cu solar cells were enhanced and demonstrated by Walter Schottky, Lars Grondahl, Neville Mott and others. Moreover, the photovoltaic effect in cadmium sulfide was discovered by Audobert and Stora. [4,5]

The first usable solar cell was made from silicon and published in 1954 by Daryl Chapin, Calvin Fuller and Gerald Pearson. In 1958 solar cells were first used in a practical application in a satellite. Since that time photovoltaics is the accepted energy source for space applications.[4,5] In the same year Hoffman Electronics achieved a solar cell efficiency of 9%. The efficiency increased to 14% in 1960 also reached by Hoffman Electronics. [5]

The production of silicon for photovoltaic applications is relatively energy-intensive, so other types of solar cells were developed, for example thin film photovoltaics. In 1980 the first thin-film solar cell exceeds 10% efficiency at the University of Delaware. This solar cell consisted of copper sulfide/cadmium sulfide. [5,6]

In 1990 Martin Green and coworkers reported a record-breaking crystalline silicon solar cell with an efficiency eventually reaching 25%. In 1991 Brian O'Regan and Michael Grätzel reported a solar cell based on nanostructured titanium oxide. [4] It is not possible to list all achievements in solar cell technology. Still worth mentioning are the discovery of a fully organic solar cell in 2001 and the application of perovskite as a sensitizer in solar cells in 2009. [5,7]

2. Principle of solar cells

In a photovoltaic device the sunlight is directly converted into electricity. So far, the solar cell science has been dominated by inorganic solid-state devices. However, the development of other types of solar cells can reduce the cost of the devices and make them more environmentally friendly. [8]

2.1. Silicon solar cell

A silicon solar cell consists of one material which is doped in two different ways and such solar cells are called single junction solar cells. The regions of a single junction solar cell are the n-type and the p-type region, called emitter and base, respectively. When light is irradiated on the solar cell the semiconductor material absorbs the photons and an exciton, which is a bound state of an electron and an electron hole, is created. In the depletion region also called space charge region the mobile charge carriers can be separated by an electronic field. The electrons are moving towards the negative pole and the holes are going to the positive pole. The excitons, which are formed out of the depletion region, can only be converted to power when the diffusion length of the electrons is long enough to reach the space charge region. When the mobile charge carriers do not reach the depletion region, they recombine and cannot be used for generating electricity. A typical silicon solar cell is shown in Figure 2. [9,10,11]

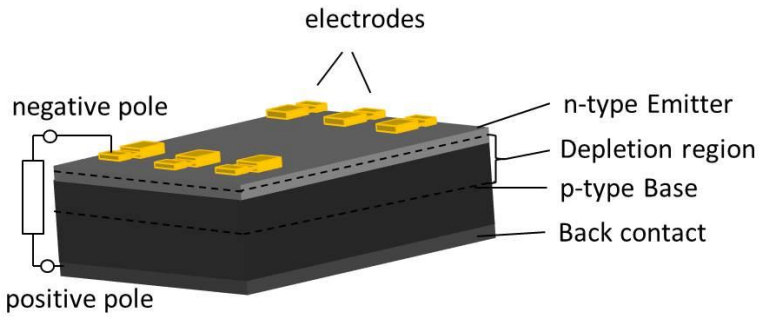

Figure 2 Silicon single junction solar cell[9]

To avoid the recombination of the charge carriers the silicon has to be very pure and crystalline, every defect in the crystal can cause recombination. Another factor affecting recombination is the surface of the silicon layer, but this cannot be avoided. [9,10,11]

2.2. Dye-sensitized solar cell (DSSC)

The dye sensitized solar cell (DSSC) was invented by Michael Grätzel and Brian O'Regan, it is also often called Grätzel cell. The DSSC consists of a nanocrystalline semiconductor oxide film electrode, a dye sensitizer, an electrolyte, a counter electrode and a transparent conduction substrate. The electrolyte, which is commonly used, is an organic or ionic liquid solvent with a solution of the I_3^-/I^- redox couple (see Figure 3). [8,12]

The working principle of the DSSC is based on the fact that under irradiation of sunlight the dye molecules become photo-excited, afterwards the dye injects an electron into the conduction band of the semiconductor and the dye is oxidized. Then the electrolyte containing I_3^-/I^- subsequently restores the original state of the dye. The redox couple is regenerated by reduction of triiodide at the counter electrode. [12, 13]

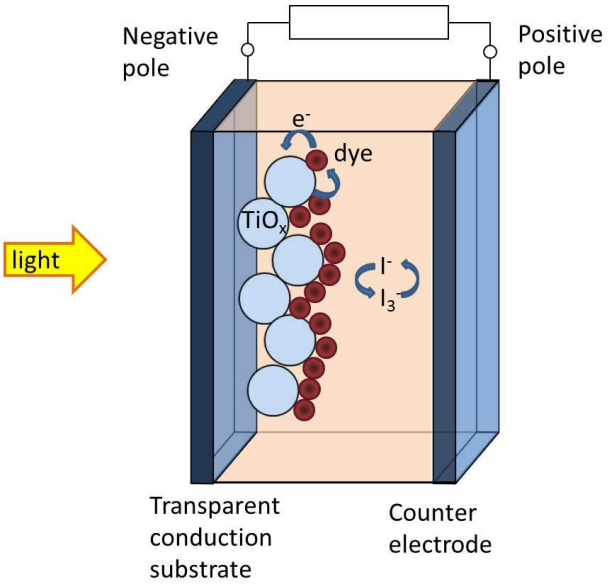

Figure 3 Dye sensitized solar cell[8]

The recombination rate in a DSSC is very low, because electrons are regained from the electrolyte to the dye at a very fast rate. Also the direct recombination from the TiO_x to the electrolyte is rather slow and the electron transfer from the counter electrode to the electrolyte is very fast. [8,13]

Due to the fact, that in the DSSC there are fewer recombinations, the solar cells are extremely efficient at converting absorbed photons into free electrons, but the power conversion efficiency is still relatively low compared to silicon solar cells. In DSSCs the rate of photon absorption is lower because typical dyes have poorer absorption in the red part of the spectrum. [13]

A big advantage of the DSSC is that low-cost materials are used and they are simple to manufacture, so it can replace the existing technologies in applications like rooftop solar collectors. Unfortunately

there are some problems with stability. Some dyes degrade when exposed to ultraviolet radiation and the use of liquid electrolytes can be a problem because they cannot be used in a high temperature range. The electrolyte can freeze at low temperatures and at high temperature it expands. [13]

The electrolyte problems can be solved when a solid state material is used instead of the liquid electrolyte. The solution can be replaced by a wide band gap semiconductor of p-type polarity, like the inorganic materials CuI and CuSCN, or organic materials, such as 2,29,7,79-tetrakis(N,Ndi-p-methoxyphenyl-amine)9,99-spirobifluorene. [12,14]

2.3. Solar cell characteristics and parameters

The I-V characteristics of a solar cell correspond in principle to the characteristics of a photodiode only the solar cell produces a photocurrent. The I-V characteristics are recorded by measuring the current during the variation of the voltage. The I-V characteristics are measured twice, once with illumination and once without. The illumination is standardized to make the solar cell performances comparable because photovoltaic devices are spectrally selective and performance measurements vary as a function of the incident spectrum, usually light with air mass 1.5 (AM 1.5) spectrum is used as a standard. Air mass refers to the relative path length of the direct solar beam through the atmosphere. The air mass is one when the sun is directly overhead (zenith). AM 1.5 is the relative path length of the sunlight through the atmosphere at a zenith angle of 48.2 °, which is the case in many of the world's major population centers. [9,15]

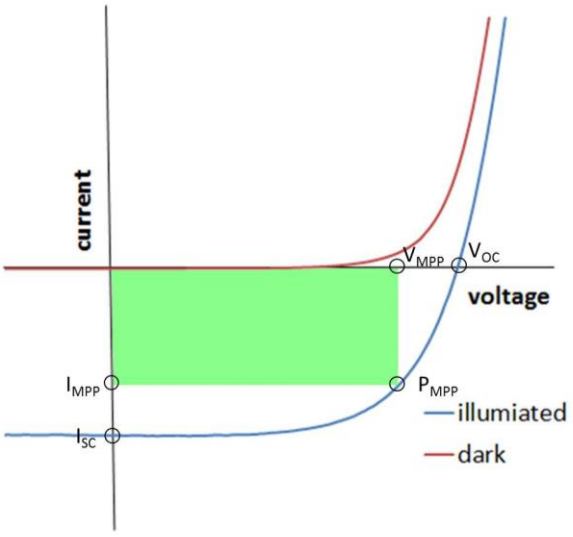

Figure 4 I-V characteristics of a solar cell[10]

Most of the photovoltaic parameters and the electric behaviour of the device can be evaluated from the I-V characteristics and some of the parameters can be read directly from the I-V characteristics,

as it is shown in Figure 4. The most important photovoltaic parameters are the open circuit voltage (V_{OC}), short circuit current (I_{SC}), fill factor (FF), maximal power point (P_{MPP}), power conversion efficiency (PCE) and the internal photon to current efficiency (IPCE).[16]

- Open circuit voltage (V_{OC})

The V_{OC} that occurs in the I-V characteristics is found at zero current. The V_{OC} corresponds to almost flat valence and conduction bands. [9,16]

- Short circuit current (I_{SC})

The maximum extracted photocurrent is the I_{SC}, it is measured when the voltage in the cell is zero. The I_{SC} depends on the illumination, which is irradiated on the cell. [9,17]

- Maximum power point (MPP)

The solar cell does not deliver the same power over the whole working area, so there is a point where the solar cell has the maximum power. The electrical power is defined by current times voltage, so that the point of the maximal power of a solar cell is the product of the V_{MPP} and the I_{MPP}. [9]

- Fill factor (FF)

The fill factor describes the ratio of the area of V_{MPP} and I_{MPP} that is the maximal power (P_{MMP}) to the area of V_{OC} and I_{SC} (see Equation 1). The FF is also a measurement for the quality of the cell and it describes the "squareness" of the I-V-curve. The limit of the FF has an ideal value of one, but the typical values for silicon solar cells are 0.75 - 0.85. For thin film solar cells the FF is mostly between 0.6 and 0.75. [9,17]

$$FF = \frac{P_{MPP}}{V_{OC} * I_{SC}} = \frac{V_{MPP} * I_{MPP}}{V_{OC} * I_{SC}}$$

Equation 1 Fill factor[17]

- Power conversion efficiency (PCE)

The PCE of a solar cell gives the percentage of the incident light which is converted into electrical power (see Equation 2).[9]

$$PCE = \frac{P_{MPP}}{P_{in}} = \frac{V_{OC} * I_{SC} * FF}{P_{in}}$$

Equation 2 Power conversion efficiency[9]

- Incident photon to current efficiency (IPCE)

At a specific wavelength λ, the yield of photogenerated electron per incident photon is the incident photon to current efficiency (IPCE) or External Quantum Efficiency (EQE). The IPCE can be calculated as shown in Equation 3. The IPCE is determined through the I_{SC}, a numerical factor, the incident power (P_{in}) and the wavelength (λ). [16]

$$IPCE = \frac{I_{SC} * 1240}{P_{in} * \lambda}$$

Equation 3 Internal photon to current efficiency[16]

3. Perovskite

Perovskite in general is a calcium titanium oxide mineral with the chemical formula of $CaTiO_3$. Gustav Rose discovered it in 1839 in the Ural Mountains. Although Gustave Rose discovered it the mineral was named after the Russian mineralogist Lev Perovski. The name "perovskite" later on was given to any material with the same type of crystal structure, so the structure of $CaTiO_3$ is now known as the perovskite structure. The perovskite structure occurs extensively in nature, for example magnesium silicate perovskite ($MgSiO_3$), which is one of the most abundant minerals in the earth's mantle. [18]

Pure perovskite compounds have the generic chemical formula of AMX_3. A is an organic or inorganic cation and M is a metal cation, these cations have very different sizes. X is an anion which binds to both cations, as shown in Figure 5. [18,19]

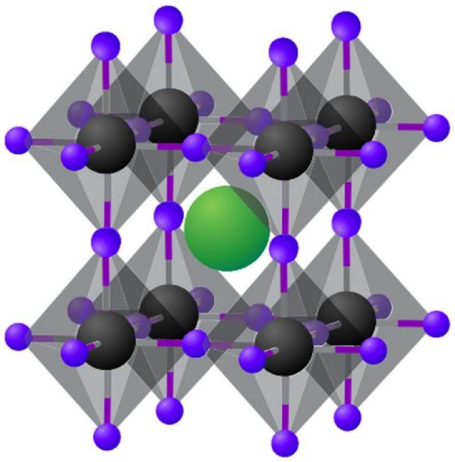

Figure 5 Crystal structure of perovskite with the generic chemical formula of AMX_3 organic or inorganic cations A (green), metal cations M (gray) and halides or oxygens X (purple)[19] **image taken from Ref [19] © by 2014 Macmillan Publishers Limited**

The perovskite structure needs a very high order and a defined relative ion size to be stable, so that many physical properties of the perovskites depend on the details of distortions and partly on the

dielectric, electronic and magnetic properties. These properties are very important for the application of perovskite material.

The different types of perovskite can be categorized in inorganic oxide perovskite and halide perovskite. This classification is shown in Figure 6. The halide perovskites can be divided into alkali-halide perovskite and organo-metal halide perovskites. The inorganic oxide perovskites can be categorized in intrinsic perovskites and doped perovskites.[18]

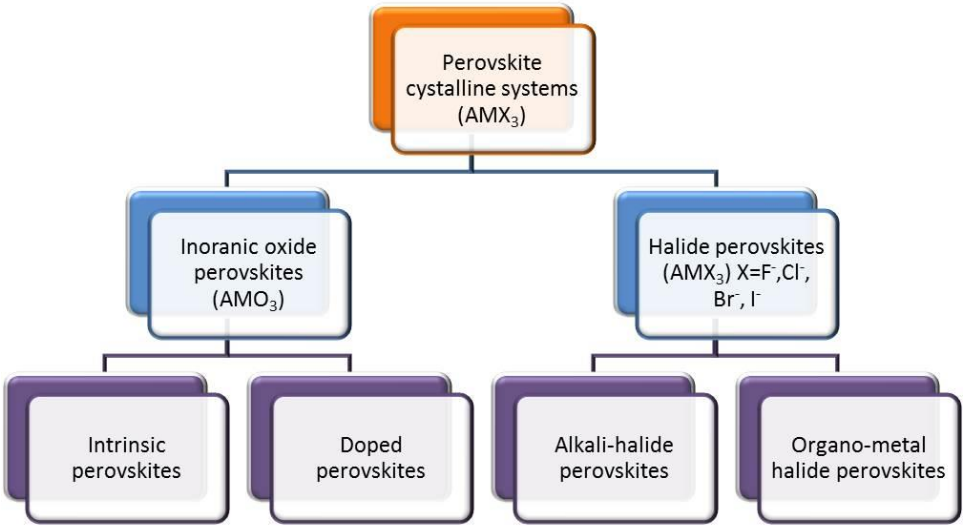

Figure 6 Crystalline perovskite systems[18]

3.1. Oxide perovskite (AMO_3)

The typical oxide perovskites are alkaline earth metal titanates, which are colourless solids. In 1956 a photocurrent was observed in oxide perovskite $BaTiO_3$ for the first time. The potential of photovoltaic application of oxide perovskite became an interesting research subject. However, the obtained efficiency was rather low, typically less than 1%. [18]

3.2. Halide perovskite (AMX_3)

The halide perovskites are a big part of the perovskite family and they can be divided roughly into alkali-halide perovskites and organo-metal halide perovskites. The alkali-halide perovskites are composed of a monovalent alkali metal cation, a divalent metal cation and a halogenide anion. In 1980 Salau reported that $KPbI_3$ has an absorption edge that matches the solar spectrum, but no real solar cell device was built based on this alkali metal halide perovskite material. [18]

The organo-metal halide perovskites consist of an organic cation such as aliphatic or aromatic ammonium cations, a divalent metal cation and a halogenide anion. The organo-metal halide

perovskite can build a 3D structure which leads to a narrowed band gap and increased mobility of charges within the layer. This photo or ionic conductivity and semiconducting properties are required in light-emitting diode and thin film transistor applications.[18]

By varying the combination of the cationic and anionic compounds a bandgap tuning can be achieved easily. From the first principle study it is known that the electronic structures, such as the valence band maximum and the conduction band minimum of the halide perovskite are dominated by the characteristics of the M-X bond. [18]Due to the fact that the organo-metal halide perovskites have very good semiconductor properties they are used as visible light sensitizers for photovoltaic cells.[18]

4. Perovskite solar cells

The first solar cells using perovskites were DSSCs using $CH_3NH_3PbX_3$ as a sensitizer. Miyasaka *et al*. reported the first perovskite solar cells with an efficiency of 3.81% ($CH_3NH_3PbI_3$). These solar cells were based on mesoporous TiO_2 photoanodes.[18,20]

Methylammonium lead iodide ($CH_3NH_3PbI_3$) is a semiconducting pigment with a direct bandgap of 1.55 eV. The absorption onset of $CH_3NH_3PbI_3$ occurs at 800 nm, making the material a good light absorber over the whole visible solar emission spectrum. [19]

The system of perovskite sensitized solar cells was further improved via optimization of the titania surface and processing of the active layer. So 6.54% power conversion efficiency was achieved, but the stability of the solar cells was very poor. Further improvements of the efficiency were made by using a solid hole transport material instead of the liquid electrolyte. M. Grätzel and co-workers achieved a PCE of 9.7%[21] with spiro-MeO-TAD as a hole transport material. This was the highest reported efficiency for solid state DSSCs at that point. The reason for the high efficiency is the strong absorbance and EQE of the perovskite over a high range.[22]

Soon after it was discovered that the mesostructured n-type TiO_2 can be replaced with an inert scaffold, such as Al_2O_3. These experiments were carried out by H. Snaith in collaboration with T. Miyasaka.[23] The results showed that the perovskite material can behave as a n-type semiconductor.[18,24] Another field of research was the HTM-free perovskite solar cell, in which the perovskite behaves as a p-type semiconductor. It was demonstrated that a simple two-component $TiO_2/CH_3NH_3PbI_3$ solar cell can function very well. The resulting perovskite solar cell differs from the original DSSC technology in many key components and can be regarded as a new and independent type of solar cells.[24]

Since the efficiency of the perovskite solar cells was improved so easily, further research was conducted. From a transistor measurement it was concluded that $CH_3NH_3PbI_3$ behaves as an ambipolar semiconductor. An ambipolar semiconductor is able to transport both electrons and holes. Because of this knowledge a perovskite solar cell with a planar geometry, meaning a cell without a mesoporous scaffold, was built. [19] Furthermore, the perovskite was used in a typical organic photovoltaic device structure with a hole blocking layer (PCBM) and an organic transparent conductor (PEDOT:PSS) as the positive charge collection contact. [18]

The preparation of the perovskite layer is the most challenging part because the perovskite structure needs a very high order to achieve the best properties. The easiest one is the one step precursor deposition. In this method the PbX_2 and the CH_3NH_3X (X= halide) were dissolved in a high-boiling solvent and coated on the substrate. With this method the morphology is hard to control and the reproducibility is poor. [18]

In order to get better control over the crystal growth the sequential deposition method was invented. In this method the PbX_2 is coated onto the devices and after annealing exposed to a solution of CH_3NH_3X. The sequential deposition method allows for a better control over the morphology compared to the one step precursor deposition. [18]

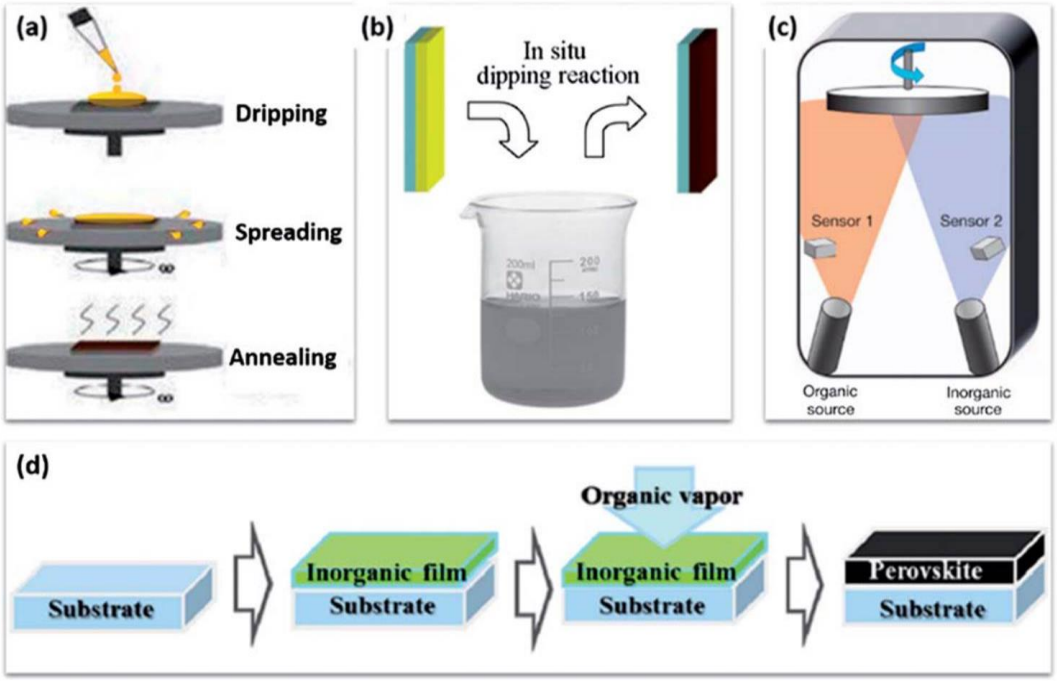

Figure 7 Methods of preparation of perovskite layers[18] (a) one step deposition method (b) sequential deposition method (c) dual source vapour deposition method (d) vapour-assisted solution process (image taken from Ref [18] © by The Royal Society of Chemistry 2014)

The dual source vapour deposition is used to prepare thin films as the absorbing layer in a planar heterojunction solar cell. The two precursor materials are evaporated and deposited on the TiO_x coated glass substrates. The advantage of the dual source vapour deposition is that the films are extremely uniform at a nanometer scale. The crystal platelets of the solution processed film were only uniform at a micrometer scale. [18] With this method an efficiency of 15.4% could be achieved by Mingzhen Liu, Michael B. Johnston and Henry J. Snaith.[25]

The vapour-assisted solution process is a combination of the sequential deposition method and the dual-source vapour deposition. In this process the PbX_2 is coated on the substrates and then annealed in a CH_3NH_3X vapour. A PCE of 12.1% was enabled in a planar architecture with this method.[26] The highest certified efficiency till today of 20.1% was reported by researchers at KRICT Institute in Daejeon, South Korea.[18]

Lead is a toxic and harmful element and because of this researchers are trying to replace it. The most likely substitute is a group 14 metal, such as tin. Although the organo-halide tin perovskite is less stable against oxidation than the organo-halide lead perovskite it was used in solar cell application by Henry J. Snaith *et a*l achieving more than 6% efficiency.[27]

The perovskite solar cells are a great opportunity to produce cheap and effective thin film solar cells. The perovskite solar cells combine the advantages of organic compounds like solution processability and optical property tunability and the advantages of inorganic crystalline semiconductors such as high charge mobility and large absorption coefficients[18].

The efficiency of perovskite solar cells will likely exceed 20% in the next few years.[19] Because they can be easily made with solution processes a simple roll to roll process is possible which leads to low production costs. The weak points of perovskite solar cells are the use of lead and the poor stability. Once a lead free perovskite with a high stability is found, perovskite solar cells will be the next great achievement in photovoltaics. Moreover, perovskite solar cells are well suited as a top cell in a tandem solar cell. The base cell could be crystalline silicon or copper indium gallium selenide. [19]

III RESULT AND DISCUSSION

1. Lead Perovskite

Great achievements in the field of perovskite solar cells were made in the last few years because of this it had become a well explored type of solar cell. First the preparation of a high efficient lead perovskite solar cell had to be found by trying to reproduce the fabrication procedures from literature.[25,28] The focus of this chapter is finding the best preparation conditions for the organo lead halide perovskite solar cells.

1.1. Heterojunction perovskite solar cells

All given solar cell parameters are the average of the best five solar cells on one device. On one device there are 20 solar cells. The size of the substrate was 24 mm x 75 mm x 1.1 mm. The solar cells were built on a glass substrate with an etched indium tin oxide surface (ITO). The substrates were washed with acetone and sonicated in isopropanol. On the oxygen plasma activated surface a compact titaniumoxide layer was coated. Sometimes a mesoporous titaniumoxide layer was deposited on the compact titaniumoxide layer. Before the active layer was coated onto the titaniumoxide the surface was again activated with oxygen plasma. Then a hole transport material was coated on the perovskite active layer. Finally a gold or silver electrode was evaporated on the substrate through a shadow mask (see Figure 8).

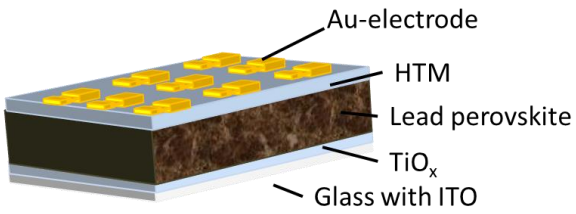

Figure 8 Solar cell architecture

1.1.1. $CH_3NH_3PbI_3$

The active layer was prepared with two different methods. The first one is a solution based method where PbI_2 and Methyl-ammonium-iodide (MAI) were dissolved in a high-boiling solvent and the perovskite was coated on the substrates. In the second method the PbI_2 was coated on the substrates and dipped in a MAI solution, so the perovskite is thereby formed on the substrate.

1.1.1.1. Solution-Method

In all experiments described below 2,2',7,7'-tetrakis(N,N-di-p-methoxyphenylamine)-9,9-spirobifluorene (Spiro-OMe-TAD) was used as a hole transport material (HTM) except for these experiments where it is mentioned that Poly(3-hexylthiophene-2,5-diyl) (P3HT) was used as a HTM.

1.1.1.1.1. Planar heterojunction perovskite solar cell

The solar cells described in this chapter were made in a planar architecture with only compact TiO_x as an underlayer.

Different preparation processes and conditions

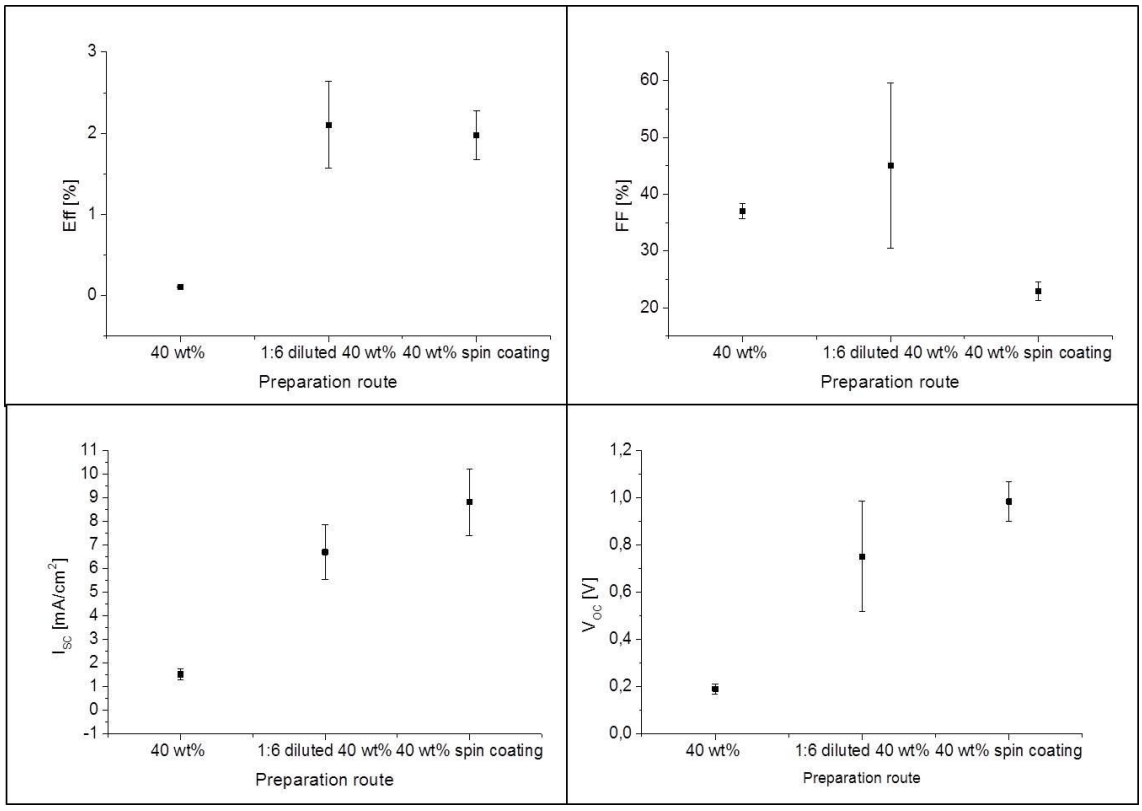

Figure 9 Comparison of different preparation routes (spin coating and doctor blading)

Glass substrate/ITO/c-TiO_x/$CH_3NH_3PbI_3$/Spiro + add/Au

In the first experiments different coating processes of the active layer were tested. First the active layer was spin coated on a compact titaniumoxide (c-TiO_x) similar to procedures described and published by e.g. Jin-Wook Lee *et. al.*[29], but no homogenous layer could be prepared. Thus it appeared that nearly the same efficiency was achieved if the perovskite layer was coated on the substrates via doctor blading with a higher dilution as reported for the spin coating (see Figure 9). In Figure 9 the comparison of different preparation routes is shown.

Spin coating the active layer results in a better I_{SC} and a better V_{OC} but because of the low fill factor the efficiency is slightly lower than the efficiency of the solar cells prepared via doctor blading. Due to the fact that the solar cells made via doctor blading with a dilution of 1:6 had the best performance in the following experiments this dilution was used for the next experiments. To investigate which doctor blading condition is the best, different temperatures and atmospheres were tested.

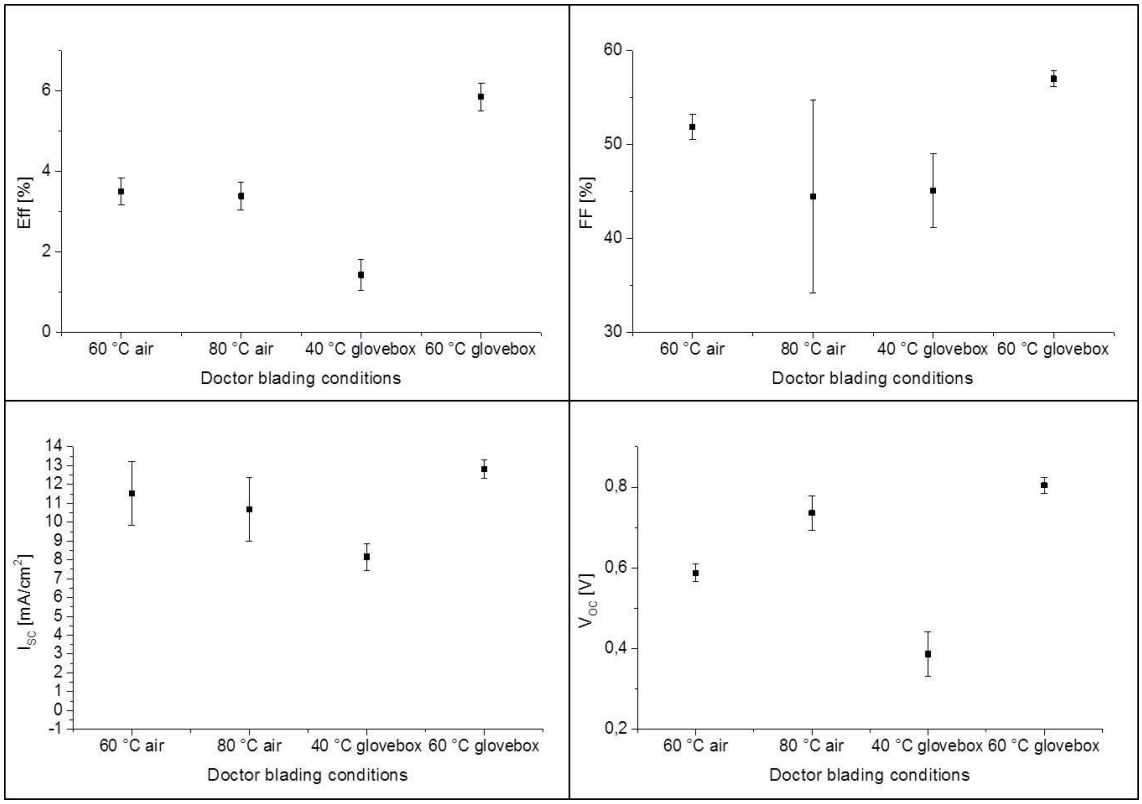

Figure 10 Comparison different doctor blading conditions

Glass substrate/ITO/c-TiO_x/$CH_3NH_3PbI_3$/P3HT + add/Au

The best doctor blading conditions were in the nitrogen filled glovebox with a temperature of 60°C (see Figure 10), this device showed the best performance in all four parameters. Due to the low heat exchange in the glovebox the temperature of 80 °C was not tried in the glovebox because it would take too long to cool it down again. The HTM used in this experiment was P3HT. The P3HT was coated via doctor blading with a speed of 25 mm/s. The thickness of the active layers was measured and was about 100 nm except for the best solar cell in this experiment. The active layer of the solar cell with the best performance was about 60 nm. The overall thickness of the solar cells with HTM was again very similar for all substrates except for the one fabricated in the glovebox at 60°C. This solar cell had a thickness of 120-200 nm and it was very smooth in comparison to the others. Maybe the thinner layer and the smoother surface of the solar cells were the reason for its better performance.

The results of the solar cells made with P3HT as a HTM were very inconsistent and could not be reproduced. Because of the thickness measuring of the active layer the solar cells were taken out of the glovebox for a short time. It was checked if this short time at ambient conditions has an effect on the solar cell performance, but no effect could be detected. Also for the thickness measurement the active layer was scratched, but the scratching of the active layer had no effect on the solar cell efficiency. Very important for the layer formation is the annealing step, therefore different annealing conditions were tested.

Different annealing conditions and influence of the top electrode

Table 1 Comparison of different annealing temperature

Glass substrate/ITO/c-TiO_x/$CH_3NH_3PbI_3$/Spiro + add/Ag

Annealing temp.	Eff [%]	FF [%]	I_{SC} [mA/cm^2]	V_{OC} [V]
120 °C	0.565 ± 0.43	37.0± 6.5	4.06 ± 0.85	0.340 ± 0.22
110 °C	0.082 ± 0.10	43.5 ± 24.5	1.08 ± 0.79	0.197 ± 0.13
100 °C	0.159 ± 0.24	36.5 ± 37.2	1.12 ± 0.67	0.571 ± 0.54
90 °C	1.24 ± 0.09	30.7 ± 3.1	5.60 ± 0.37	0.728 ± 0.06

The next step was to find the best conditions for the annealing of the perovskite layer. In Table 1 it is shown that the solar cells with an annealing temperature of 90 °C showed a better performance than these annealed at 100 °C, although 100 °C is a very common annealing temperature in literature.[29,30] The highest fill factor was achieved with an annealing temperature of 110°C. This annealing temperature experiment was carried out with silver as a top electrode. In the following experiments it was found, that the solar cells with a gold electrode showed higher efficiencies. Therefore this was repeated with gold as a top electrode, but it showed the same results. In all following experiments the perovskite layer was annealed at 90°C.

Silver could not be evaporated on the substrate reproducibly. Thus, many of these solar cells were short circuited and some acted as if there were contact problems or dendrites were formed through the layer, whereas with gold as the top electrode such problems did not occur. Due to these results, the top electrode of all following devices was gold.

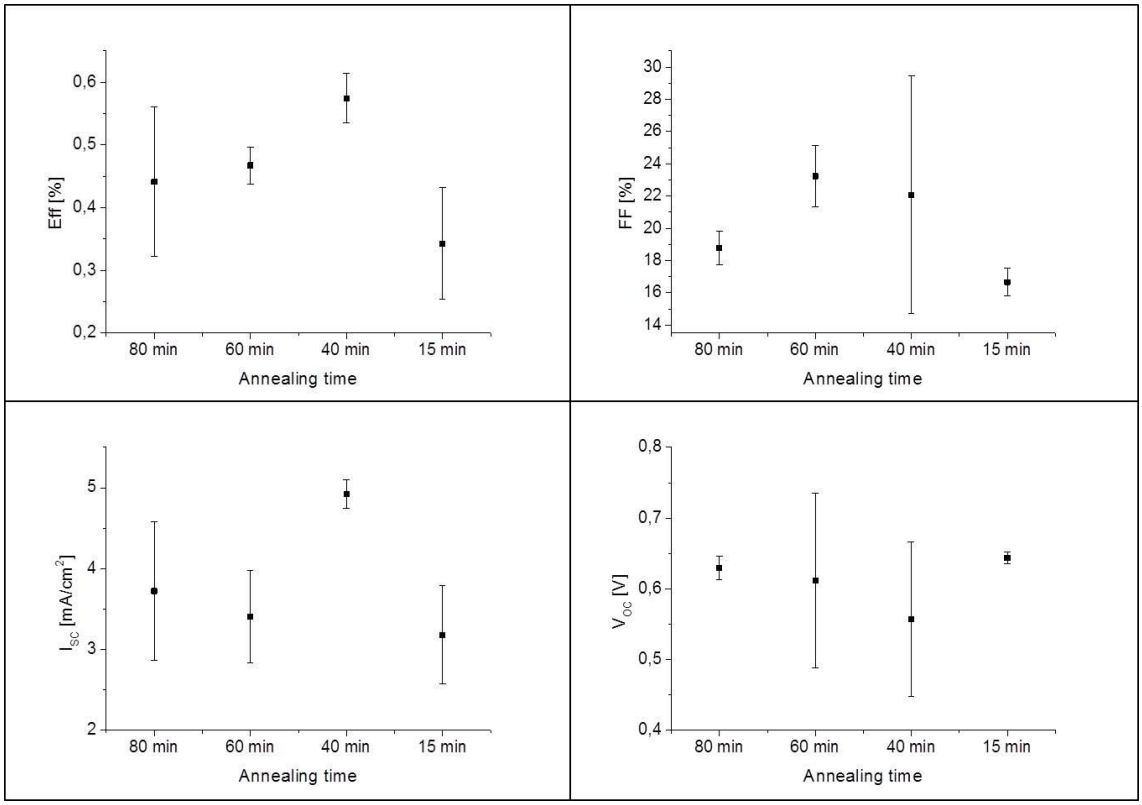

Figure 11 Comparison of different annealing times

Glass substrate/ITO/c-TiO_x/$CH_3NH_3PbI_3$/Spiro + add/Au

Many different annealing conditions were reported in the literature, so that different annealing times had to be tested, to find the best conditions. As it is shown in Figure 11 the best efficiency and the highest I_{SC} appeared at an annealing time of 40 minutes. At this annealing time the fill factor and the V_{OC} showed a very high standard deviation although the I_{SC} and the efficiency had a low standard deviation. The highest fill factor was achieved at an annealing time of 60 min, but it had a low I_{SC}. Due to the fact that the solar cells with an annealing time of 40 min had the best efficiency (see Figure 11) this annealing time was used for the following experiments. According to the presented results 40 min and 90 °C are the best crystallization conditions for the lead perovskite prepared by the solution method. Another important influence on the active layer is the concentration and the solvent of the coating solution that is why these parameters were varied next.

Different coating solution parameter

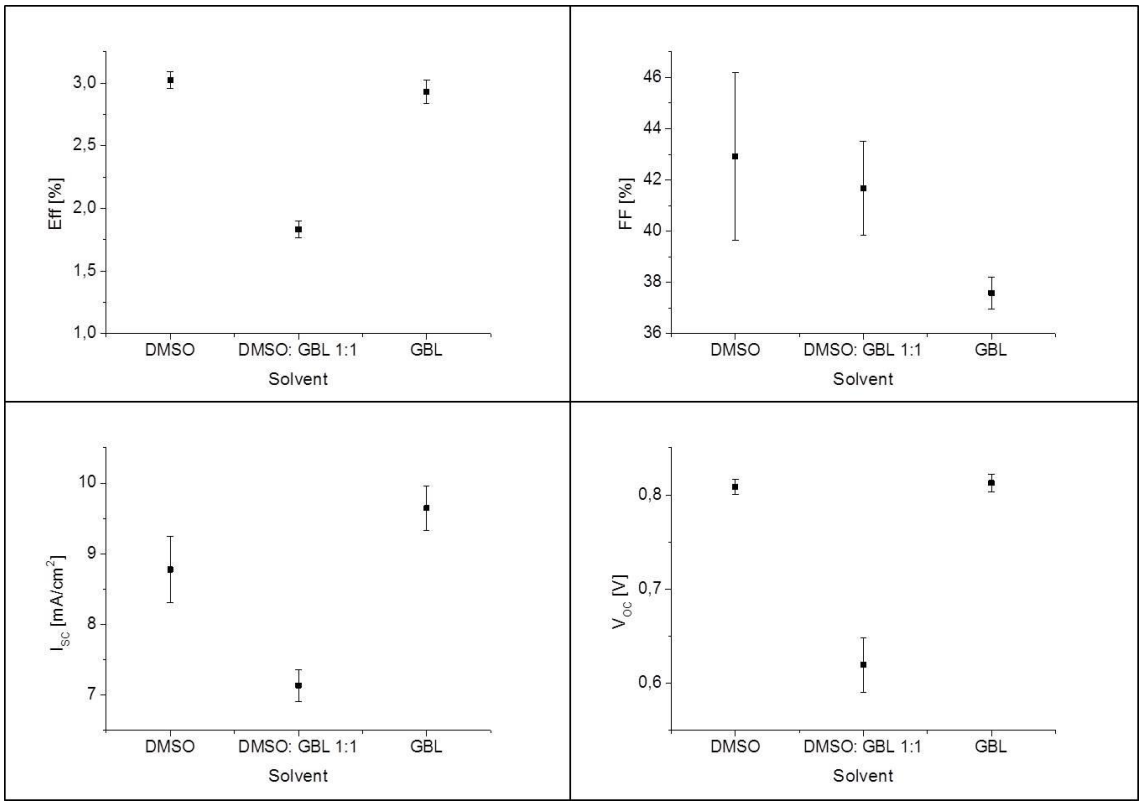

Figure 12 Comparison of different solvents (DMSO, GBL and a mixture of these two)

Glass substrate/ITO/c-TiO_x/$CH_3NH_3PbI_3$/Spiro + add/Au

Different high-boiling solvents for the fabrication of perovskite solar cells are described e. g. by Nam Joong Jeon and coworkers[31]. To see which solvent achieves the best performance, the perovskite solution was made with different solvents (Dimethylsulfoxid (DMSO), γ-butyrolacton (GBL) and a mixture of these two). The comparison of the solvents showed that the solar cell fabricated with DMSO had the best efficiency, so that in the following series DMSO was used. DMSO was also used in the previous experiment as a solvent. The perovskite solar cells dissolved in GBL had nearly the same performance as DMSO. As in Figure 12 the I_{SC} of GBL was higher than the one with DMSO and the V_{OC} was nearly the same, but the fill factor was very low. The solar cells prepared with the solvent mixture solution had the worst performance.

The idea of the solvent mixture was taken from literature[31]. In this publication the perovskite layer is also treated with toluene to get an extremely uniform and dense layer. It was tested if there is an improvement of the solar cell performance with a toluene treatment. The active layer was dried at 60 °C and then toluene was coated via doctor blading on top after this the layer was annealed as usual. It occurred that sometimes there was no effect on the solar cell performance. Therefore no toluene was used in the following experiments. Another factor

which influences the crystallization of the active layer is the layer thickness. The layer thickness can be influenced via modifying the concentration of the perovskite solution.

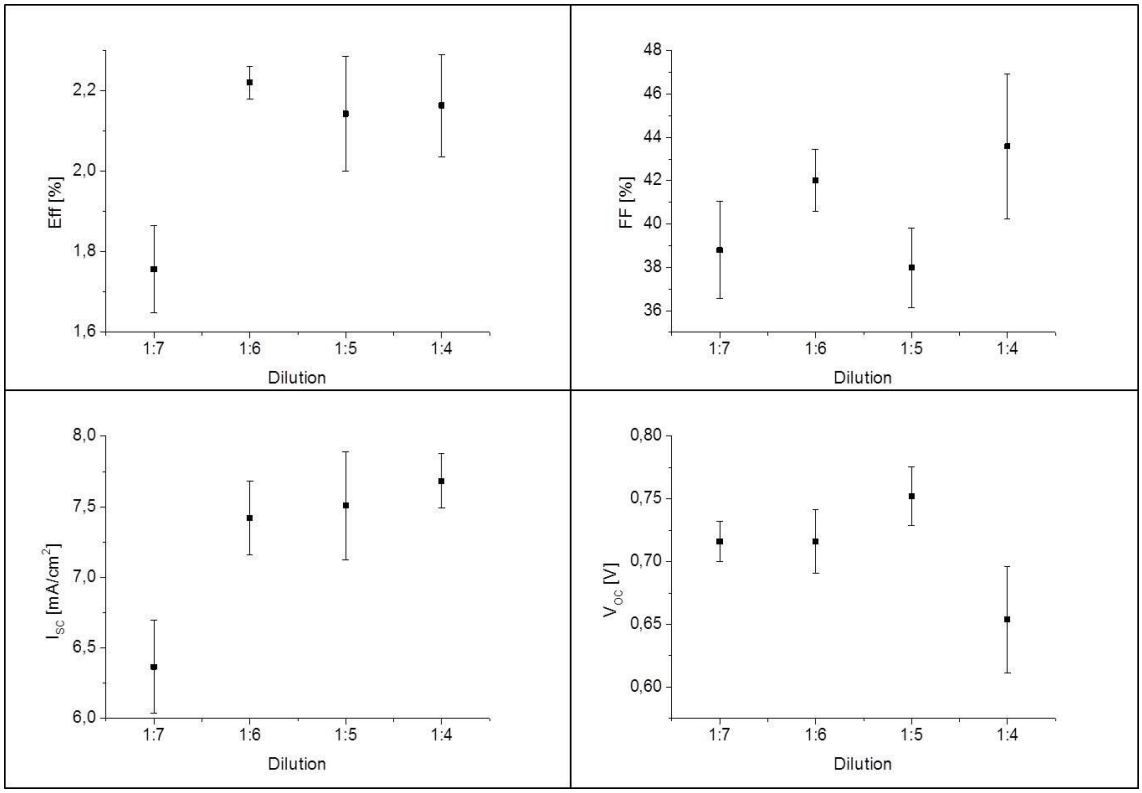

Figure 13 Comparison of different dilutions

Glass substrate/ITO/c-TiO_x/$CH_3NH_3PbI_3$/Spiro + add/Au

In the next experiment a closer look was taken on the concentration of the perovskite-solution in DMSO. The concentration of the perovskite solution was 92 mg/mL (1:7), 105 mg/mL (1:6), 122 mg/mL (1:5) and 147 mg/mL (1:4). The values in the parenthesis give the respective dilution of the 40 wt% stock solution. As shown in Figure 13 the devices with 1:6, 1:5 and 1:4 dilutions had a good efficiency, but the 1:6 dilution had the highest average efficiency and the lowest standard deviation. The I_{SC} is increasing with decreasing dilution, the V_{OC} is also increasing with higher concentration, but only till a dilution of 1:5. The dilutions 1:6 and 1:5 had nearly the same performance, but trends of several experiments indicated that the fill factor with a dilution of 1:6 is a little bit higher than with a dilution of 1:5. The variation of the concentration of the perovskite solution had a big influence on the layer thickness. The layer thicknesses of the solar cells (active layer + HTM) were 350 nm ± 2.2 nm (1:7), 408 nm ± 2.0 nm (1:6), 435 nm ± 1.3 (1:5) and 423 ± 6.0 nm (1:4). The perovskite layers with a higher concentration were more turbid because of the thicker layer and the roughness of the solar cells increased with the concentration. The results suggest that the best layer formation occurs with a dilution of 1:6. Also the stirring time of the perovskite solution made a difference on the

efficiency of the solar cells. Nevertheless, it is hard to say which stirring time is the best, but it is in a range of 60 - 84 h.

1.1.1.1.2. Mesostructured heterojunction perovskite solar cells

The previous described experiments were all made on a c-TiO_x blocking layer. In the literature a mesoporous titaniumoxide (mp-TiO_x) is often used. To find the best conditions for a mp-TiO_x underlayer most experiments made with c-TiO_x were repeated with a mp-TiO_x underlayer. The mp-TiO_x was formed on top of the c-TiO_x. For the mp-TiO_x a TiO_x-paste DSL 30 NRD purchased from Dyesol was used. To find the perfect layer thickness the TiO_x-paste was diluted 1:3.5 weight ratio in ethanol as it is published in literature[32]. To find the right viscosity for doctor blading the mp-TiO_x layer the 1:3.5 pre-diluted TiO_x-paste was further diluted in ethanol. The best performance was found at a pre-diluted TiO_x-paste dilution of 1:1 volume ratio with ethanol. In all following experiments mp-TiO_x was used.

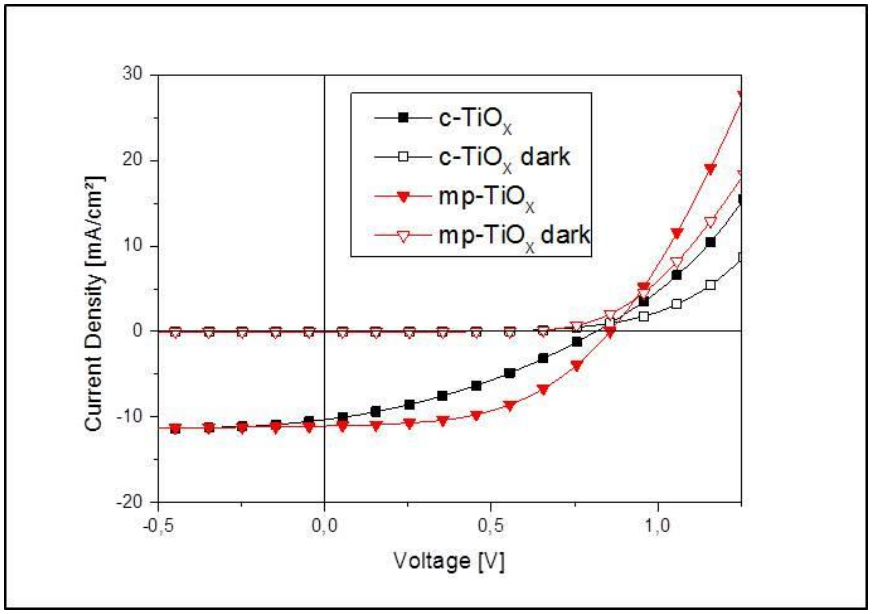

Figure 14 I-V characteristics of perovskite solar cells on compact TiO_x and on mesoporous TiO_x Glass substrate/ITO/c-TiO_x or c-TiO_x and mp-TiO_x/$CH_3NH_3PbI_3$/Spiro + add/Au

The difference between the compact underlayer and the mesoporous underlayer is shown in Figure 14. The efficiency of the solar cell on mp-TiO_x diagrammed in Figure 14 was 4.72% and that of the solar cell on c-TiO_x was 2.87%. Generally the solar cells on mp-TiO_x had a better performance than the solar cells on c-TiO_x. The solar cell on mp-TiO_x had a better fill factor and a higher V_{OC} (see Figure 14). The I_{SC} of the c-TiO_x solar cell is a little bit lower than that of the solar cell on mp-TiO_x, this may be caused by the lower fill factor.

The hole transport material (HTM) can have a big effect on the performance of a perovskite solar cell. Therefore two different HTM were tested.

Different hole transport materials

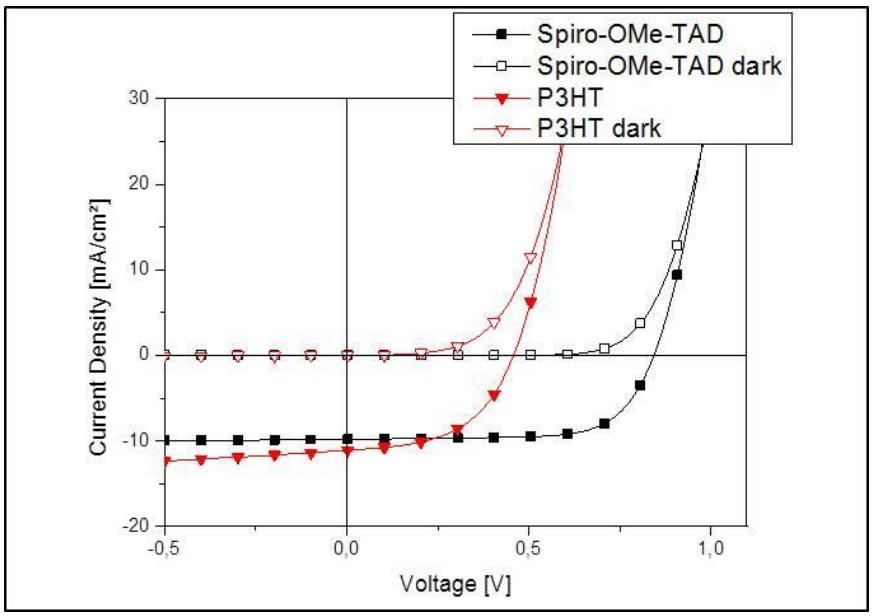

Figure 15 I-V characteristics of solar cell with Spiro-OMe-TAD and P3HT as HTM

Glass substrate/ITO/ c-TiO_x/mp-TiO_x/$CH_3NH_3PbI_3$/Spiro + add or P3HT + add/Au

To make clear which HTM had the better performance Spiro-OMe-TAD and P3HT were both used in one experiment on two different devices. In Figure 15 the best solar cell of one device is shown. The devices only differed in the HTM-layer. As it is shown in Figure 15 there is a big difference between the two hole transport materials. The V_{OC} of the solar cells with Spiro-OMe-TAD was nearly twice as high as the V_{OC} of the solar cells with P3HT. The I_{SC} is nearly the same in both cases, only the best cell with P3HT had a better I_{SC} than the best cell with Spiro-OMe-TAD. The average I_{SC} of the solar cells with Spiro-OMe-TAD is a little bit higher than the average I_{SC} of the solar cells with P3HT. The Spiro-OMe-TAD cells had a very good fill factor of nearly 70%. The efficiencies of the solar cells shown in Figure 15 were 5.75% (Spiro-OMe-TAD) and 2.61% (P3HT). The layer thickness of the solar cell with Spiro-OMe-TAD is about 460 nm, that for the solar cell with P3HT it is about 300 nm. The thickness difference could only be caused by the HTM layer. The thinner P3HT layer may be the reason for the voltage losses in the P3HT solar cell. Another possibility for the decreased voltage are pinholes within the P3HT layer.

With both HTMs different layer thicknesses were tested. To get a thicker Spiro-OMe-TAD layer a higher concentration was used, but the performance of the solar cells decreased. It was also attempted to affect the layer thickness with the doctor blading speed, but it showed no big

effect on the performance of the solar cell. The best performance was achieved with a concentration of Spiro-OMe-TAD of 72.3 mg/mL and a doctor blading speed of 20 mm/s, so a layer thickness of approximately 200 nm was achieved. Solar cells with P3HT had the best performance with a P3HT concentration of 15 mg/mL and a doctor blading speed of 20 mm/s. A layer thickness of approximately 120 nm was achieved under these conditions.

Different annealing conditions and solution parameters

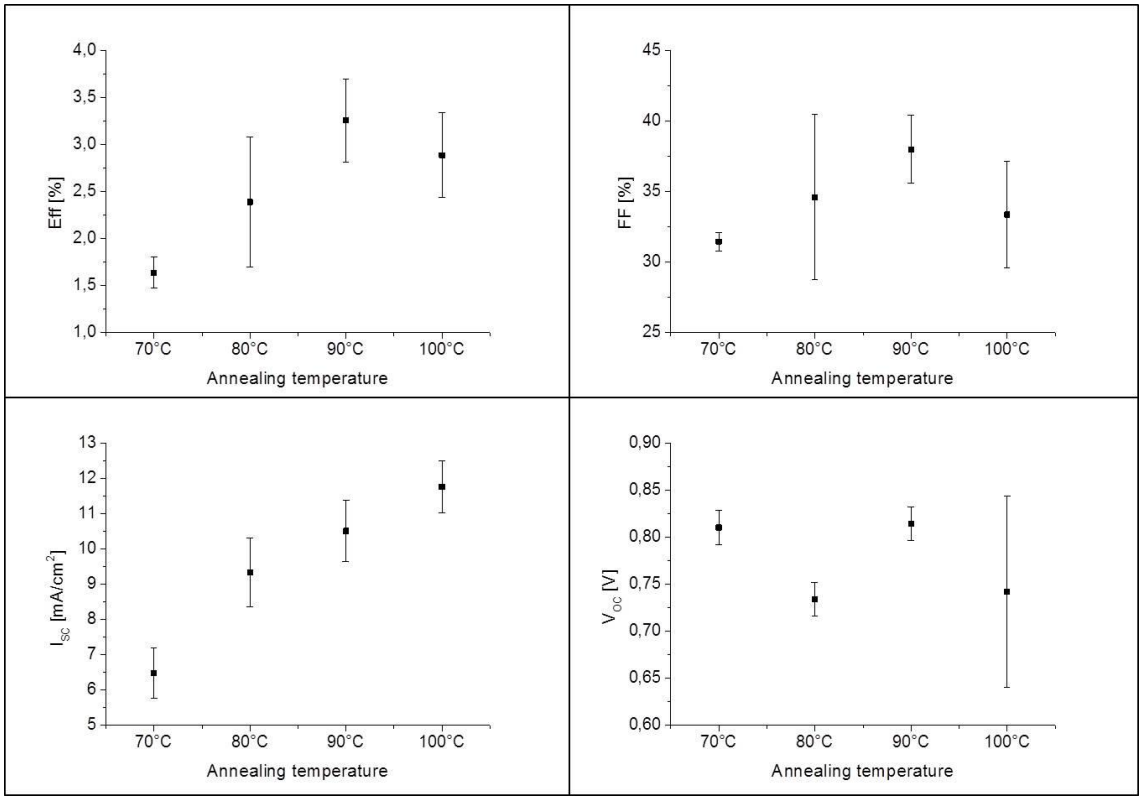

Figure 16 Comparison of different annealing temperature on mp-TiO_x

Glass substrate/ITO/ c-TiO_x/mp-TiO_x/$CH_3NH_3PbI_3$/Spiro + add/Au

To make sure that the best condition of annealing and the best solution parameter of the active layer have not changed because of the mesoporous underlayer some experiments were repeated. First of all different annealing temperatures on the mp-TiO_x were tested (see Figure 16). In the annealing temperature experiment on compact TiO_x the solar cell annealed at 90 °C had the best performance. It appeared that again 90 °C had the best performance. Only the I_{SC} was higher at an annealing temperature of 100 °C. The I_{sc} is decreasing with decreasing annealing temperature. The other three parameters had the best performance at an annealing temperature of 90 °C.

Different concentrations of the perovskite solution were also tested on mp-TiO_x. The 40 wt% stock solution was diluted 1:7, 1:6, 1:5 and 1:4 to get different concentrations.

Table 2 Solar cell parameter of different concentration of the perovskite solution in DMSO on mp-TiO_x

Glass substrate/ITO/ c-TiO_x/mp-TiO_x/$CH_3NH_3PbI_3$/Spiro + add/Au

Dilution	Eff [%]	FF [%]	I_{SC} [mA/cm^2]	V_{OC} [V]
1:7	0.090 ± 0.01	59.7 ± 3.73	0.288 ± 0.04	0.531 ± 0.06
1:6	3.2 ± 0.37	50.7 ± 1.87	8.75 ± 0.38	0.718 ± 0.06
1:5	3.1 ± 0.15	53.4 ± 4.04	8.32 ± 0.68	0.694 ± 0.01
1:4	2.0 ± 0.17	42.4 ± 3.72	7.63 ± 1.18	0.644 ± 0.04

The different dilutions in DMSO of the perovskite on mp-TiO_x showed very different performances (see Table 2), but the best one was again the solar cell with a dilution of 1:6, it had the best efficiency, highest I_{SC} and highest V_{OC}. Only the fill factor stepped out of line, the highest fill factor had the solar cell with a dilution of 1:7 which had over all a very bad performance. The I_{SC} and the V_{OC} increased with higher dilution up to a dilution of 1:6. Thus, it appeared that are no big changes in the behaviour of the lead perovskite on a c-TiO_x or a mp-TiO_x scaffold. The layer thicknesses of the solar cells (active layer + HTM) were 521 ± 24 nm (1:7), 411 ± 18 nm (1:6), 464 ± 23 nm (1:5) and 540 ± 34 nm. The layer thickness increases with the concentration of the precursor solution only the lowest concentration had a thicker layer that expected.

Ageing effect of the solar cells

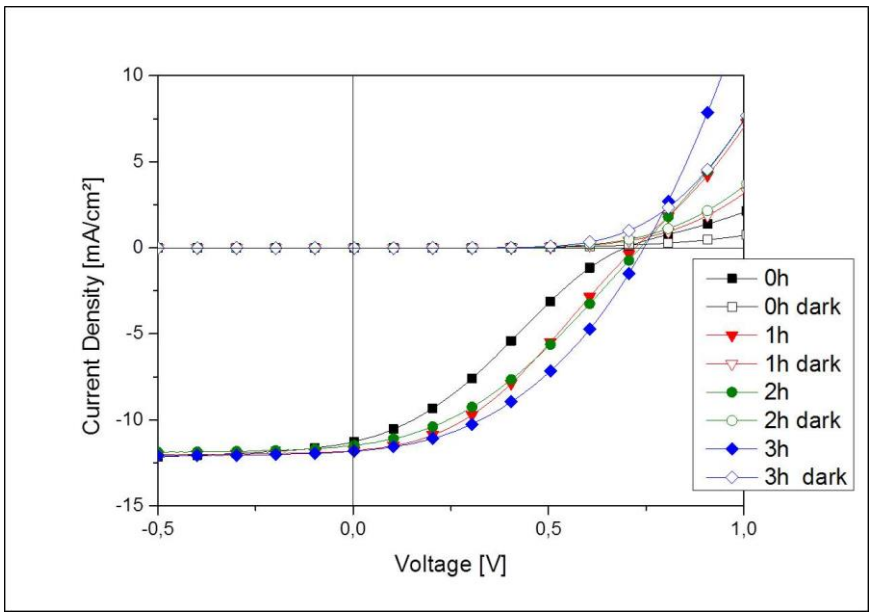

Figure 17 I-V characteristics of one device to demonstrate the ageing of the solar cell

Glass substrate/ITO/ c-TiO_x/mp-TiO_x/$CH_3NH_3PbI_3$/Spiro + add/Au

It appeared that the solar cells had an ageing effect (see Figure 17). Maybe the improvements are based on light soaking processes[33] because the cells were illuminated for 15 minutes every time before measuring. As it is shown in Figure 17, especially the fill factor increases with the storage time, because of this also the I_{SC} and the V_{OC} increased a little. But there is a point where the degradation prevailed and the solar cell performance decreased. This point is hard to find because it is different for each device, but it is in the range of around 24 h.

1.1.1.2. Dipping-Method

In the dipping-method the active layer was prepared in two steps. First the PbI_2-solution was coated via doctor blading onto the substrates followed by an annealing step. After cooling to room temperature the device was dipped into a solution of 10 mg/mL CH_3NH_3I in isopropanol for 20 seconds. The perovskite structure is created during this dipping step. Finally the device was annealed again.

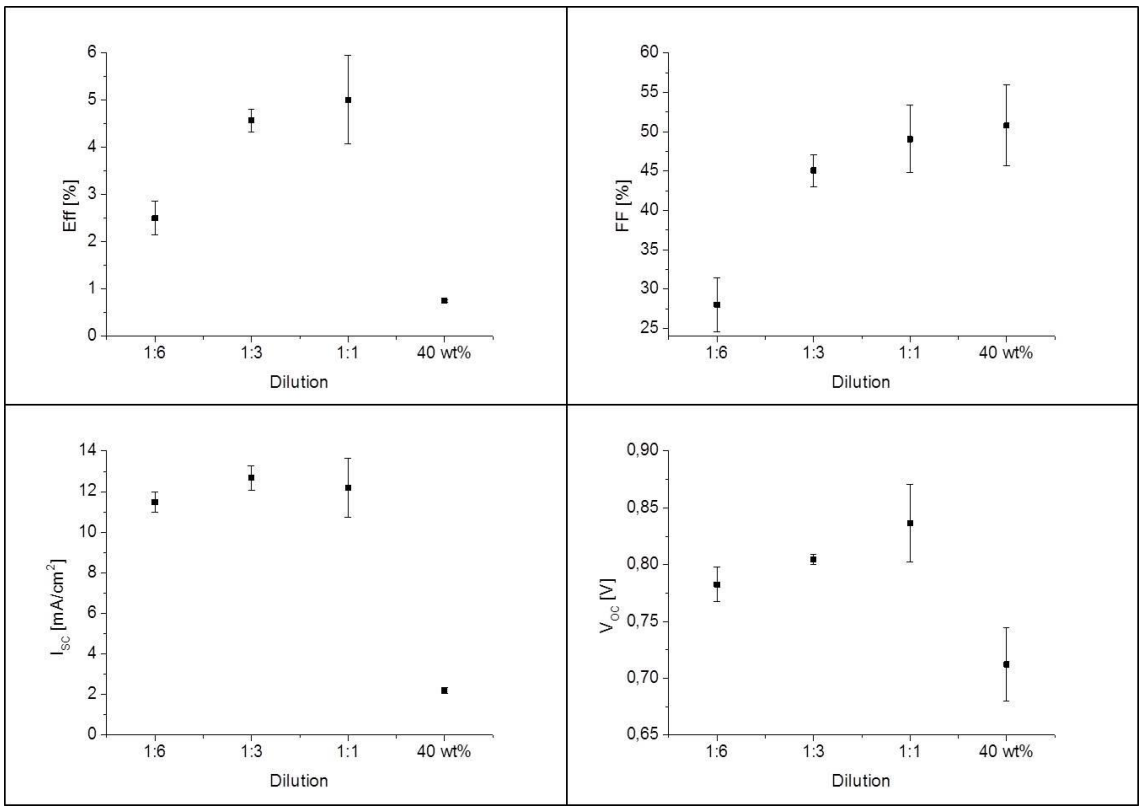

Figure 18 Comparison of different dilutions in DMF with the dipping-method

Glass substrate/ITO/ c-TiO_x/mp-TiO_x/$CH_3NH_3PbI_3$/Spiro + add/Au

To adapt the method from the literature[32] the 462 mg/mL PbI_2 stock solution in DMF was diluted to get a good result via doctor blading. The same experiment was carried out with DMSO as a solvent, but the performances were not as good as with DMF. The trends of the different dilutions were the same with both solvents. As shown in Figure 18 the fill factor is increasing with the concentration, but the I_{SC} was very low at the highest concentration. So it

appeared that the solar cell with the dilution of 1:1 volume ratio had the best efficiency and the highest V_{OC} and so over all the best performance. To determine the difference in the solar cell characteristics between the two active layer preparation methods both were fabricated in one experiment.

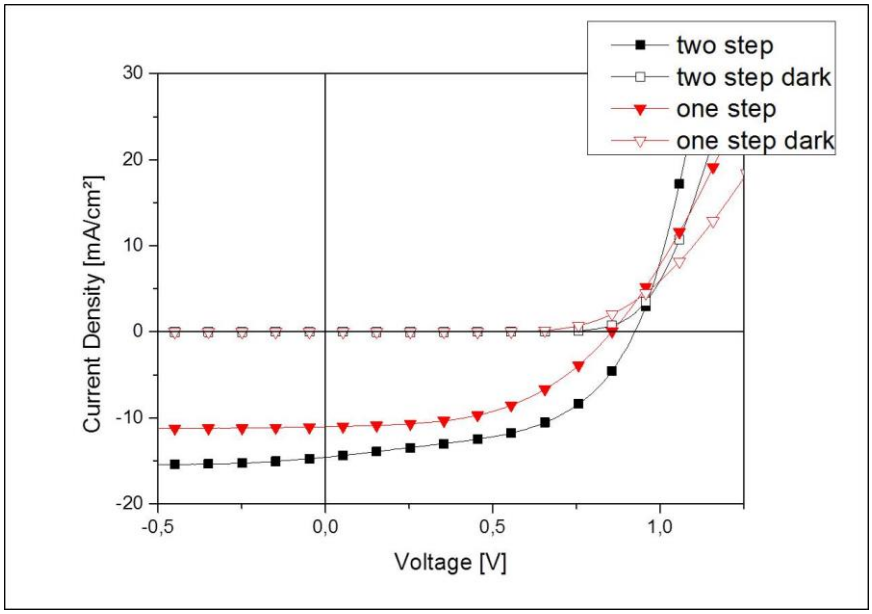

Figure 19 I-V characteristics of solar cells one active layer prepared via solution method (one step) and one via dipping method (two step)

Glass substrate/ITO/ c-TiO_x/mp-TiO_x/$CH_3NH_3PbI_3$/Spiro + add/Au

As shown in Figure 19 better performances were achieved with the dipping method. The solar cells with the I-V-characteristics shown in Figure 19 were fabricated in one fabrication step, so that there were no differences in other parameters, which could affect the performance of the solar cells. The differences between the performances of the two manufacturing methods could be based on the different layer thicknesses. With the solution method approximately 500 nm could be achieved with the dipping method up to 650 nm could be realized. Due to the unequal layer thicknesses the dipping method layer is darker than the solution method layer (see Figure 20). The thicker active layer can absorb more light, so the dipping method had a higher I_{SC}. Moreover, the dipping method solar cell also had a higher V_{OC} and because of this a higher performance. Nevertheless, as shown in Figure 20 the solution method layer is more homogeneous than the dipping method layer. This is also reflected in the higher standard deviation of the solar cells prepared with the dipping method. The relative standard deviations are 1% and 3% for the solution method and for the dipping method, respectively.

Figure 20 Solar cells solution method (left) dipping method (right)

1.1.2. $CH_3NH_3PbI_{3-y}X_y$(X=Cl or (SCN))

To test if other lead halogenides could reach a better performance lead chloride and a lead pseudohalogenide $(SCN)^-$ were used instead of lead iodide to prepare a solar cell via dipping method. All three halogenides were prepared in one fabrication run with DMF as solvent for the doctor blading step.

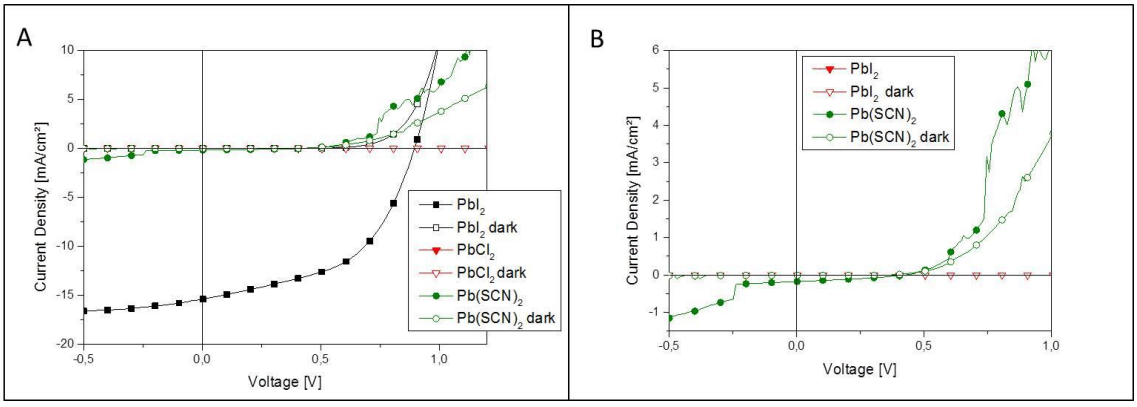

Figure 21 I-V-characteristics of solar cell with different lead halogenides (PbI_2, $PbCl_2$, $Pb(SCN)_2$) (A), only $PbCl_2$ and $Pb(SCN)_2$ (B)

Glass substrate/ITO/ c-TiO_x/mp-TiO_x/$CH_3NH_3PbI_{3-y}Xy$(X=Cl, (SCN))/Spiro + add/Au

As shown in Figure 21 the device with PbI_2 reached the best efficiency, the other solar cells did not work well, especially the one with $PbCl_2$. In Figure 21 B the pseudohalogenide and chloride are shown again without PbI_2. In Figure 21 B it could be seen that the solar cell with $Pb(SCN)_2$ showed something similar to diode characteristics. To see if a good working solar cell could also be built with $(SCN)^-$, it was tried to prepare solar cells with the solution method with $Pb(SCN)_2$ instead of PbI_2 with different ratios of $Pb(SCN)_2$:MAI (see Figure 22).

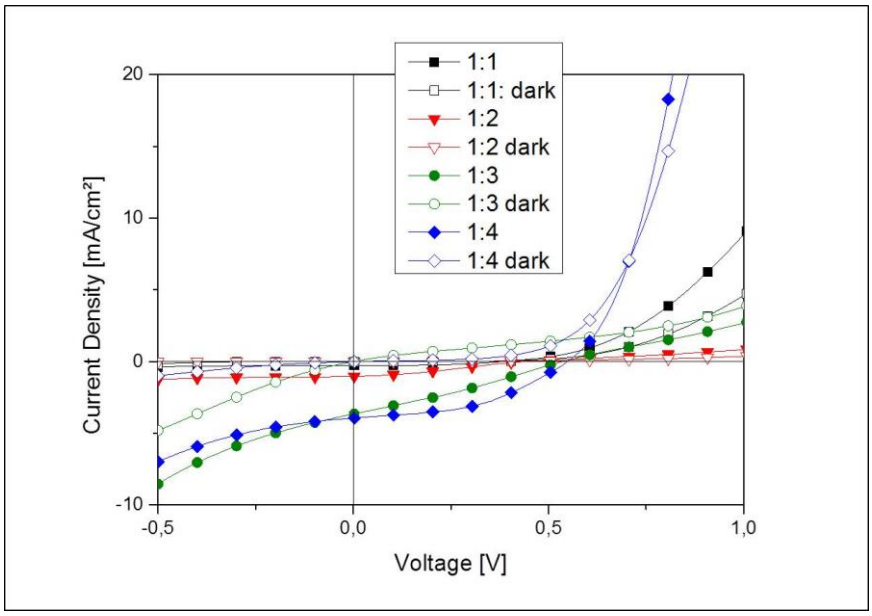

Figure 22 I-V characteristics of solar cells with different $Pb(SCN)_2$:MAI ratio
Glass substrate/ITO/ c-TiO_x/mp-TiO_x/$CH_3NH_3PbI_{3-y}(SCN)_y$/Spiro + add/Au

As it is shown in Figure 22 the performance of the solar cell increases with the $Pb(SCN)_2$:MAI ratio, this might be an indication for a replacement of the $(SCN)^-$ by I^- in the perovskite structure. The difference between the $Pb(SCN)_2$:MAI ratio 1:3 and 1:4 is only the better fill factor for 1:4, which leads to a better V_{OC} and I_{SC}.

1.2. Perovskite/PCBM Planar-Heterojunction Solar Cells

To see if there is a better performance of the perovskite in an organic assembling a solar cell on PEDOT:PSS and with PCBM was built. The solar cells were also based on a glass substrate with an etched ITO on it. These substrates were washed with acetone and sonicated in isopropanol. A PEDOT:PSS layer was spin coated on the oxygen plasma activated surface, which was dried at 150 °C for 15 min. The active layer, a solution of PbI_2 and MAI, was coated via doctor blading or spin coated on the PEDOT:PSS and annealed afterwards. For the hole blocking layer a solution of PCBM in chlorobenzene was coated on the substrates and aluminium was used as top electrode. In this assembling the current flow is reversed compared to the devices described before.

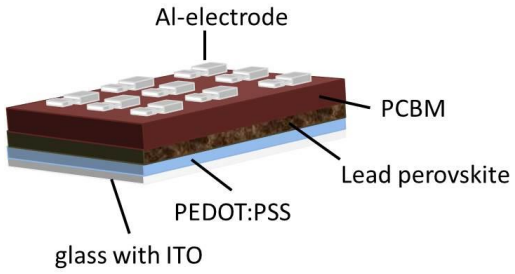

Figure 23 Perovskite/PCBM planar heterojunction solar cell architecture

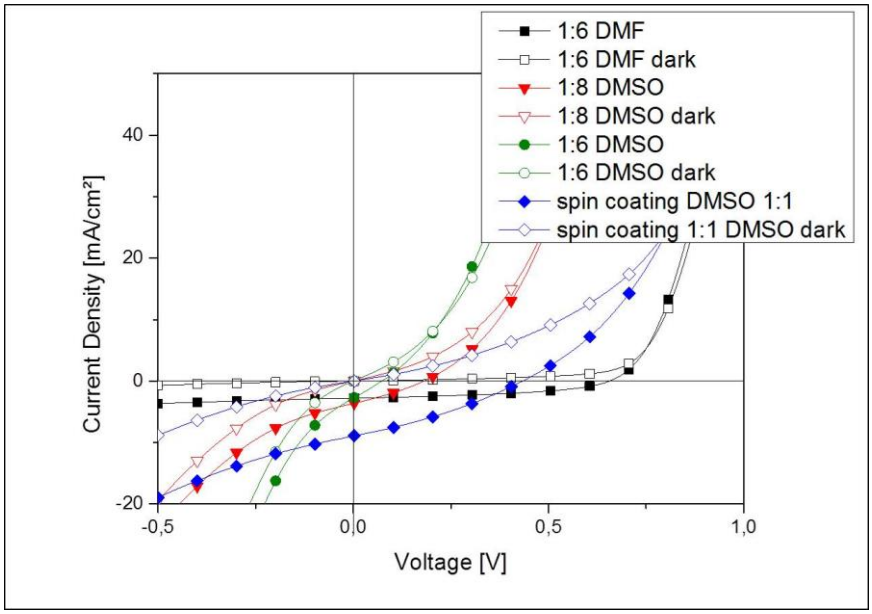

Figure 24 I-V characteristic of solar cell with PCBM

Glass substrate/ITO/ PEDOT:PSS/ $CH_3NH_3PbI_3$/PCBM/Al

Table 3 Solar cell parameter of different manufacturing ways of solar cells with PCBM

Glass substrate/ITO/ PEDOT:PSS/ $CH_3NH_3PbI_3$/PCBM/Al

	V_{OC} [V]	I_{SC} [mA/cm²]	FF [%]	Eff [%]
Spin coating DMSO 1:1	0.435	8.91	31.6	1.22
Doctor blading DMF 1:6	0.656	2.79	45.4	0.83
Doctor blading DMSO 1:8	0.183	3.60	29.8	0.20
Doctor blading DMSO 1:6	0.073	2.70	26.8	0.052

The active layers of the solar cells shown in Figure 24 were annealed for 2 hours as it is described in literature.[34] The concentration of the PCBM was 20mg/mL for the solar cells, which were fabricated via doctor blading and 15mg/mL for the solar cells, which were built via spin coating. In Table 3 the parameters of the solar cells shown in Figure 24 are listed. The spin coated solar cell had the best performance, both the PCBM layer and the active layer were spin coated on the substrate for this solar cell. The devices were cut in pieces for the spin coating because of the big size of the devices no homogenous layer can be formed otherwise. For the other solar cells the PCBM layer and the active layer were coated via doctor blading. The four solar cells shown in Figure 24 are the best solar cells of each device. It was also tried to spin coat other concentrations, but the active layer from a DMF solution was so crystalline that the layer became inhomogeneous, so that these devices did not work at all. The solar cell with an undiluted solution of DMSO had also a very bad performance, so it is not shown. As it is shown in Table 3 the solar cell prepared via doctor blading with the DMF solution had the

highest V_{OC} and a high fill factor, but a low I_{SC} so that the efficiency is not as high as for the spin coated solar cell. Nevertheless, the perovskite/PCBM solar cells did not work as well as the perovskite solar cells in the TiO_x/perovskite/HTM assembling.

1.3. Characterization

To get a deeper understanding of the processes in the solar cells, the solar cells and the perovskite layer were analysed in detail.

1.3.1. X-Ray Diffraction

To investigate if the desired perovskite structure was formed on the substrates, a XRD was measured. For these measurements PbI_2 and MAI were dissolved in DMSO, coated via doctor blading on a glass substrate and annealed for 40 min at 90 °C.

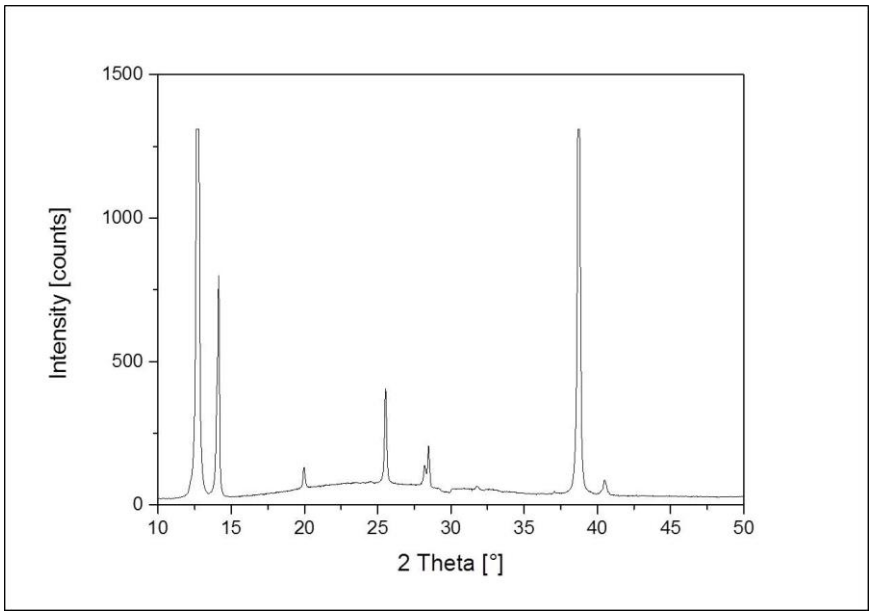

Figure 25 XRD pattern of lead perovskite on glass (measured by Birgit Kunert)

Figure 25 shows the XRD pattern of the $CH_3NH_3PbI_3$ layer prepared on glass. The highest reflections in the diffractogram belong to the hexagonal 2H polytype PbI_2[32]. The signals at 12.7 ° (0 0 1), at 25.5 ° (0 0 2) and at 38.7 ° (0 0 3) belong to the unreacted PbI_2. The other signals in the diffractogram belong to the perovskite structure. The perovskite can crystalize in different modifications and these can be differentiated in the XRD pattern. One difference is the position and the amount of signals between 27.5 ° and 31 °. The modification of the probe is tetragonal I4/mcm according to the literature[35] because there are two signals between 27.5 ° and 30 °. The lattice planes according to the reference[36] are (1 1 0) at 14.15 °, (2 0 0) at 19.98, at $(0\ 0\ 4)_\tau$ 28.2 °, at $(2\ 2\ 0)_\tau$ 28.48 °, (3 1 0) at 31.75 ° and (2 2 4) at 31.75 ° and are typical for a perovskite structure. So the XRD indicated that there is a lot of unreacted PbI_2 in the

layer. The reason for this could be that the layer was made on a flat surface in this case glass as reported in reference[32] if that is the case the PbI_2 should be less on the mp-TiO_2 or it could be a layer thickness effect as reported in reference [37].

1.3.2. UV-Vis spectra

To see if there is any difference in the optical properties of different lead perovskite solar cells UV-Vis spectra were measured. In most measured absorption spectra the absorption never goes down to zero due to interferences within the layers.

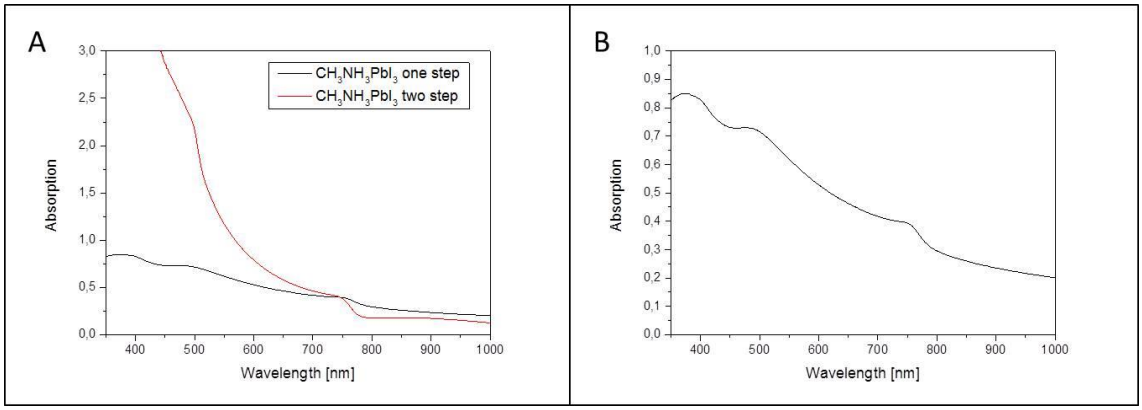

Figure 26 UV-Vis spectra of the lead perovskite layer on glass made with solution method (one step) (A and B) and dipping method (two step) (A)

The absorption spectra of the different active layer preparation methods are shown in Figure 26. The optical properties of the two manufacturing processes are the same, but the steeper increase in absorption of the layer made with the dipping method could be a matter of thickness and concentration. As evidenced in Figure 26 the absorption maximum for the solution method is located at a wavelength of 371-373 nm. With the dipping method the layer gets thicker, so the maximum of the dipping method is not clear, because the absorption is so high that the detector is saturated. The position of the maxima of the absorption spectra correlates with the position of the maxima in the literature[36], this reference also indicates that the difference in the two processing methods is only thickness dependent.

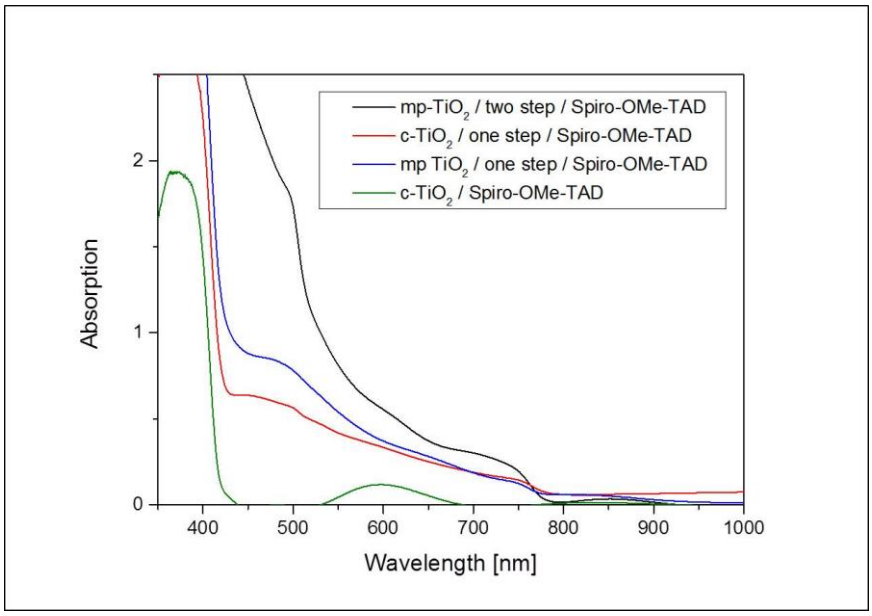

Figure 27 UV-Vis spectra of solar cells made on mp-TiO_2 and on c-TiO_2 with solution method (one step), dipping method (two step) and without active layer; all had Spiro-OMe-TAD as HTM

In Figure 27 are absorption spectra from different solar cells pictured. There is a difference in absorption because of different underlayers and because of the fabrication method. Furthermore, for comparison the absorption of a solar cell fabricated without an active layer is shown. The solution method solar cells had the same fabrication parameters only the underlayer was different. The shift of the shoulder at 491 nm (two step) to 481 nm (one step) must be caused by the mesoporous titaniumoxide or by the modification of the perovskite layer on mesoporous titaniumoxide. The solar cells had a very high absorption so detector saturation occurred. Only the absorption maximum of the TiO_x/Spiro-OMe-TAD reference could be detected at a wavelength of 375 nm.

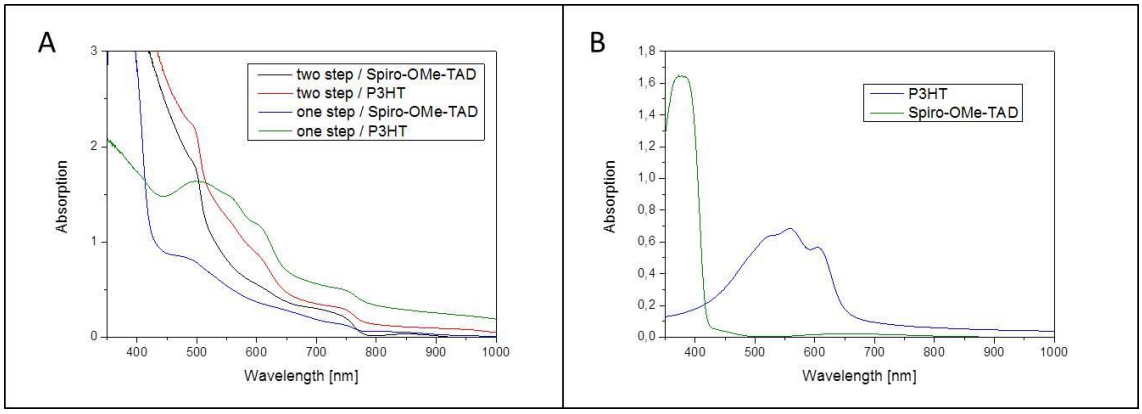

Figure 28 UV-Vis spectra of solar cells made with solution method (one step) and dipping method (two step) with Spiro-OMe-TAD or P3HT as HTM (A) and the UV-Vis spectra of the HTMs on glass (B)

To see the influence of the HTM on the absorption of the solar cell, solar cells with different HTMs and fabrication methods of the HTMs on glass were measured. The absorption of the

HTMs on glass is very different (see Figure 28). This is reflected in the absorption spectra of the solar cells. In the absorption of the solar cells made with the solution method the difference is clearer than in the absorption of the dipping method solar cells. The solar cell with the P3HT as HTM showed the hump of the P3HT absorption at approximately 500-600 nm and the solar cells with the Spiro-OMe-TAD showed the highest absorption at 350-400 nm because the absorption of the HTM and the lead perovskite overlayed. The absorption maximum of P3HT was at 556 nm and of Spiro-OMe-TAD was at 377 nm. The measured absorptions spectra correlate very well with the spectra given in the literature[38,39].

1.3.3. External Quantum Efficiency

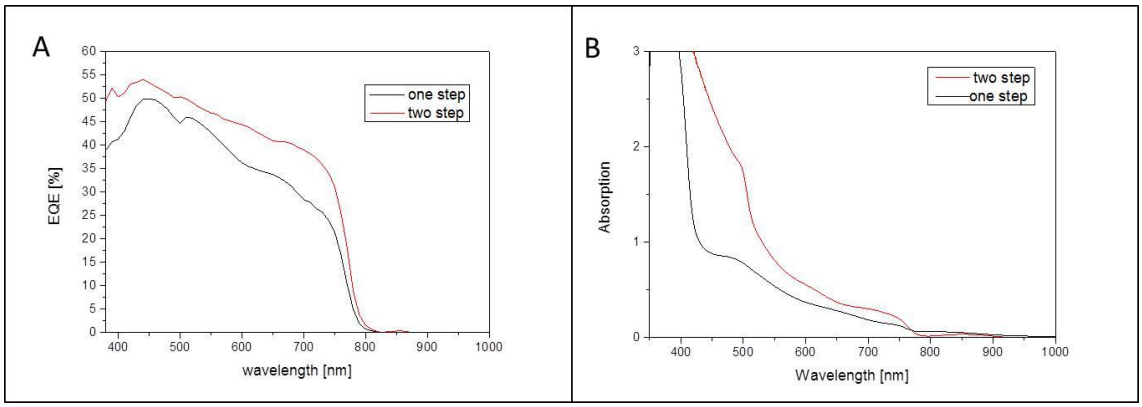

Figure 29 EQE of solar cells one made with solution method (one step) one with dipping method (two step) (A) and UV-Vis spectra of solar cells one made with solution method one with dipping method (one step) (B)

The external quantum efficiency (EQE) measurements showed a high conversion rate of photons in the solar cell (see Figure 29). The solar cells convert photons nearly over the whole visual range. In comparison to the absorption spectra the maximum shifted from approximately 372 nm to 440-450 nm, this shows that the HTM which was Spiro-OMe-TAD (absorption maximum approximately 375 nm) did not contribute anything to the generation of charge carriers.

1.3.4. Optical Band gap

The optical band gap was determinded by ploting $(\alpha h\nu)^2$ againest the energy hv and extrapolate the straight line, so the intersection point with the x-axis is the optical band gap. This way of ploting is also called Tauc plot[40].

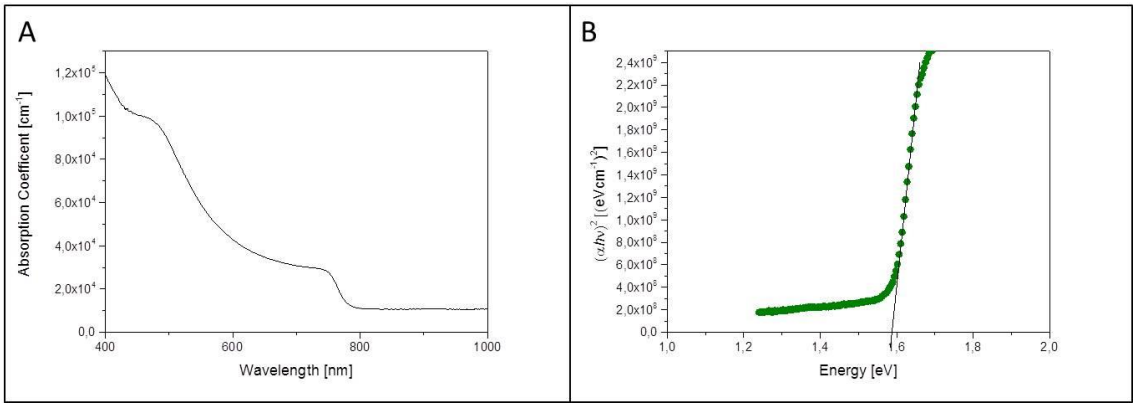

Figure 30 Absorption coefficient and band gap determination of lead perovskite

The optical band gap of the lead perovskite is 1.58 eV as it is shown in Figure 30 (B). This value suits very well to the reported values in the literature of 1.55[41], 1.57[42] up to 1.6[35]. The absorption of the lead perovskite begins at approximately 800 nm as shown in Figure 30 (A). The reason why the measurement did not start with absorption of zero may be interferences within the layers.

1.3.5. Scanning Electron Microscopy

The cross section scanning electron microscopy (SEM) images shown on the left side were taken with a topography detector (TD), the ones on the right side were taken with a material contrast detector (MCD). In the picture taken with the MCD the lighter parts are heavier elements and darker parts are lighter elements. The solar cells were built on a glass substrate with ITO on it. The next layer is the compact TiO_x layer on this layer there is the active layer. In Figure 31 and Figure 32 the active layer is infiltrated in a mp-TiO_x. On the active layer there is the HTM layer and on the top a gold electrode. In all SEM-images it can be seen that the Spiro-OMe-TAD which was used as HTM had a lot of holes within the layer and that the c-TiO_2 layer is homogenous and around 40 nm thick. To see the differences between the two active layer fabrication methods and between the different underlayers SEM images of these solar cells were taken.

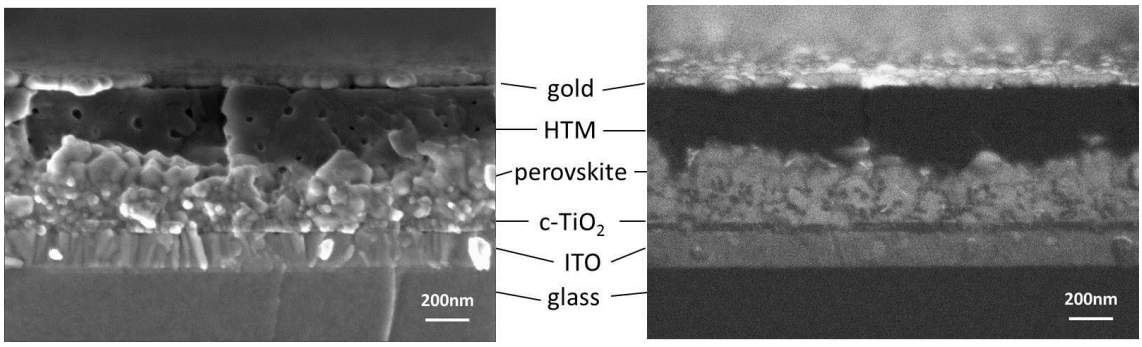

Figure 31 SEM image of a complete photovoltaic device made with dipping method (by FELMI TU Graz) topography detector (left) and material contrast detector (right)

In Figure 31 is shown the SEM image of a solar cell made with the dipping method. In Figure 32 can be seen the SEM image of a solution method solar cell. The SEM images of the two solar cells look very different. The dipping method cells had a thinner HTM than the solution method cells.

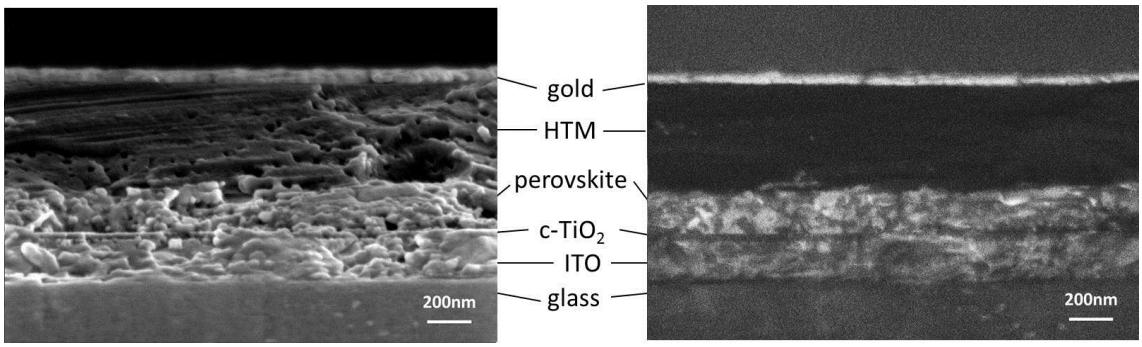

Figure 32 SEM image of a complete voltaic device made with solution method (by FELMI TU Graz) topography detector (left) and material contrast detector (right)

The solution method solar cell on mp-TiO_2 had a thin perovskite layer, but in contrast to the solution method solar cell on c-TiO_2 the layer thickness was equal at every measured spot. As it is shown in Figure 32 the solution-mp-TiO_2-solar cell had a homogenous distribution of the perovskite and the HTM layer.

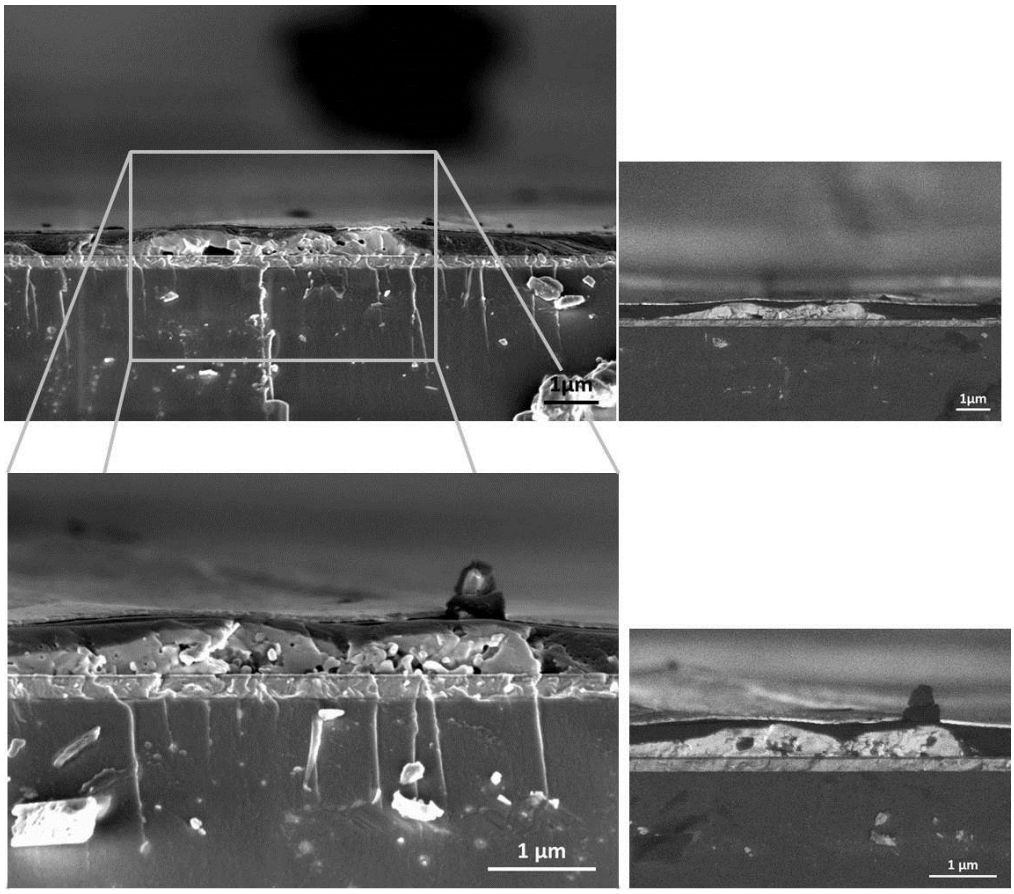

Figure 33 SEM images of a complete photovoltaic device made with solution method on c-TiO_2 (by FELMI TU Graz) topography detector (left) and material contrast detector (right)

In the solar cell on c-TiO_2 the active layer is very inhomogeneous at some spots it looked like there is not any active layer at all. Then at other places there seems to be no HTM between the active layer and the gold electrode (see Figure 33), but in some parts the thickness of the layers was almost eqaul (see Figure 34). This inhomogeneity could be a reason for worse performance of the photovoltaic device on c-TiO_2 compared to the photovoltaic device on mp-TiO_2.

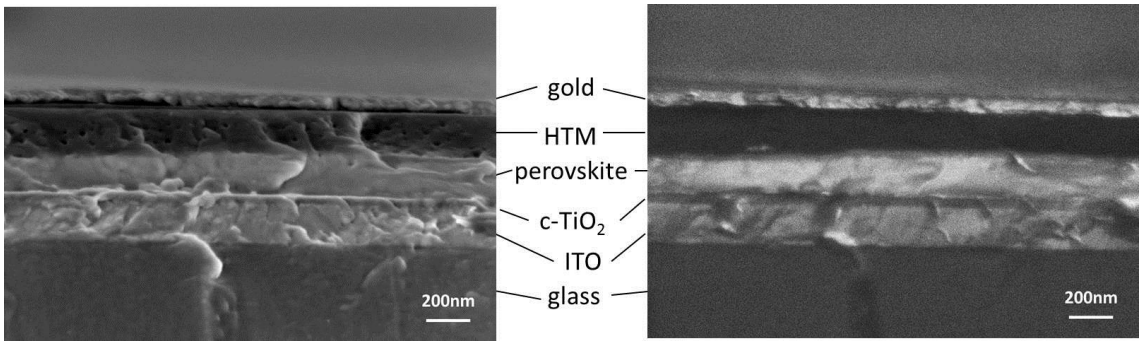

Figure 34 SEM image of a complete photovoltaic device made with solution method on c-TiO_2 (by FELMI TU Graz) topography detector (left) and material contrast detector (right)

1.4. Conclusion

To investigate the best fabrication conditions for the lead perovskite solar cells different manufacturing methods, solvents, concentrations and annealing conditions were tested. Besides different top electrode materials, different hole transport materials and different underlayers were examined. The active layer was prepared in two ways. The first method was the solution method. For this method PbI_2 and MAI were dissolved in a high-boiling solvent and coated on the substrates. The second method, which was tested, was the dipping method. In this method the PbI_2 was dissolved in a high-boiling solvent and coated on the substrate and then dipped in a MAI solution. The optimal conditions for solar cell fabrication with the solution method were doctor blading at 60 °C in the N_2-filled glovebox a 1:6 diluted 40 wt% stock solution in DMSO on mesoporous TiO_x. The best active layer annealing conditions were 40 min at 90 °C, the HTM which delivered the best performance was Spiro-OMe-TAD and with gold as the top electrode no conduction problems occurred.

Higher efficiencies were achieved with the dipping method, where PbI_2 is coated via doctor blading under the same condition as the solution method but the annealing is different. The active layer is annealed twice before and after dipping into a solution of MAI in isopropanol for 30 min at 70 °C. The solar cell with the best efficiency of 8.6% had a V_{OC} of 0.887 V, an I_{SC} of 16.0 mA/cm² and a FF of 61.0%. The assembling with PCBM/perovskite showed a lower efficiency although for one device all layers were spin coated as it is described in the literature[43].

The EQE of the lead perovskite solar cell was up to 54% at approximately 440 nm for the solution method and approximately 50% at 450 nm for the dipping method. This is in line with the measured UV-Vis spectrum. The optical band gap is 1.58 eV which matches perfectly with the band gap reported in the literature[42].

The XRD measurements confirmed that the PbI_2 and the MAI crystallize in a perovskite structure, but in an assembling with a compact underlayer some unreacted PbI_2 remained. In the SEM images the difference between the solar cells fabricated with the solution method and the dipping method was perceptible. The solar cell made with the solution method had a thinner active layer and a thicker HTM layer than the solar cell made with the dipping method. It could also be seen that the layer thicknesses of the HTM and the active layer in the planar solar cell was very inhomogeneous.

2. Lead-free Perovskite

Because lead is a poisonous heavy element and PbI_2 which could be formed when the $CH_3NH_3PbI_3$ comes in contact with polar a solvent such as water[19] harms the environment. Another problem is the "lead-free directive" which the RoHS is often inaccurately called, is the restriction of usage of lead in electrical and electronic equipment[3]. So there are doubts to put lead perovskite solar cell in commercial use. Therefore a replacement of the lead perovskite with a non-toxic alternative was attempted.

2.1. $CH_3NH_3SnI_3$

To get a lead free solar cell the lead perovskite was replaced with tin perovskite. Kanatzidis et al.[44] and Snaith et al.[27] showed that more than 6% efficiency are possible with tin perovskite solar cells. The optimized fabrication conditions for the lead solar cells were used for the first experiment only PbI_2 was replaced with SnI_2. Unfortunately an investigation of the fabrication conditions for the tin perovskite was necessary for improvement. First of all different underlayers were tested. For the tin perovskite a thicker mp-TiO_x was deposited on the c-TiO_x because the ticker mp-TiO_x showed fewer short circuits in the solar cell. Then a smooth active layer had to be prepared, so two 40 wt% solutions of SnI_2 and MAI were made in DMSO or DMF and coated at different temperatures. The results indicated that the DMF is the better choice for $CH_3NH_3SnI_3$, because some of the I-V-curves of the DMF solar cell had a diode characteristics. Nevertheless, all devices only had non-working cells, some were short-circuit and some did not let any current pass or there was only very less current flow. The active layer looked well when it was not annealed at all so that the annealing was skipped. In the next experiment the solution was diluted and it was found that the 1:6 diluted cells had the best performance. It was also tried to get a better active layer if diiodooctane is added to the solution, but that did not work out.

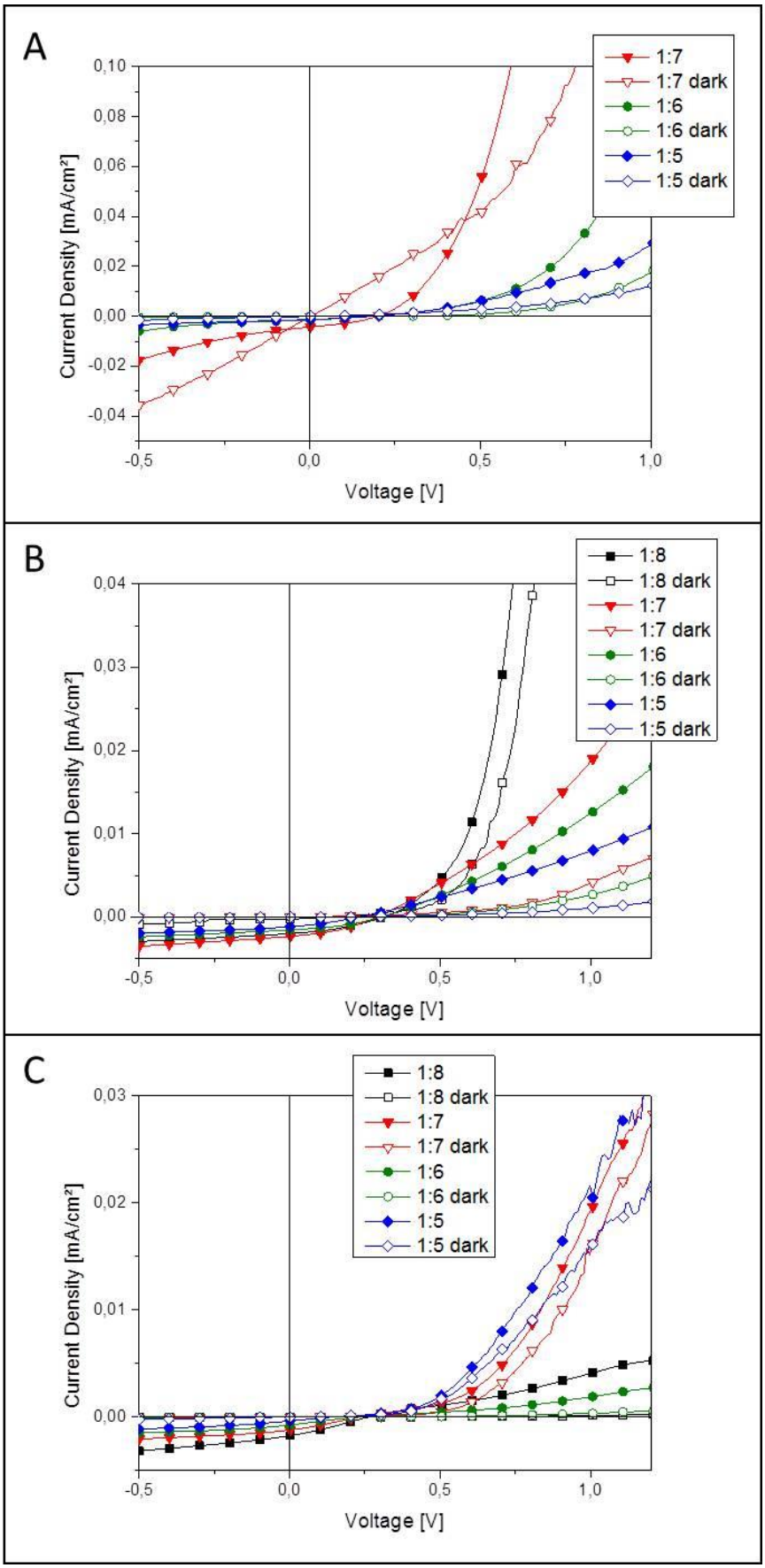

Figure 35 I-V characteristics of solar cell with $CH_3NH_3SnI_3$ A solution one day old B solution two days old C solution three days old

Glass substrate/ITO/ c-TiO_x/mp-TiO_x/$CH_3NH_3SnI_3$/Spiro + add/Au

Table 4 Solar cell parameter of solar cells with $CH_3NH_3SnI_3$ from solutions with differing ageing times

Glass substrate/ITO/ c-TiO_x/mp-TiO_x/$CH_3NH_3SnI_3$/Spiro + add/Au

Age of the solution	dilution	Eff [%]	FF [%]	I_{SC} [mA/cm^2]	V_{OC} [V]
one day	1:7	$2{,}95 * 10^{-4}$	34,1	$4{,}27 * 10^{-3}$	0,204
	1:6	$7{,}53 * 10^{-5}$	29,4	$1{,}40 * 10^{-3}$	0,183
	1:5	$6{,}88 * 10^{-5}$	29,4	$1{,}28 * 10^{-3}$	0,183
two days	1:8	$2{,}26 * 10^{-4}$	36,0	$1{,}99 * 10^{-3}$	0,314
	1:7	$2{,}53 * 10^{-4}$	37,2	$2{,}33 * 10^{-3}$	0,294
	1:6	$1{,}81 * 10^{-4}$	38,1	$1{,}56 * 10^{-3}$	0,304
	1:5	$8{,}54 * 10^{-5}$	31,2	$1{,}18 * 10^{-3}$	0,234
three days	1:8	$1{,}30 * 10^{-4}$	28,2	$1{,}75 * 10^{-3}$	0,264
	1:7	$8{,}09 * 10^{-5}$	28,1	$1{,}22 * 10^{-3}$	0,234
	1:6	$4{,}18 * 10^{-5}$	23,9	$7{,}50 * 10^{-4}$	0,234
	1:5	$1{,}28 * 10^{-5}$	24,2	$3{,}72 * 10^{-4}$	0,143

To see if the aging of the 40 wt% stock solution had any influence on the solar cell performance it was intended to prepare solar cells from the same solution on different days (see Table 4 and Figure 35). All $CH_3NH_3SnI_3$ solar cells until now have been built on a mp-TiO_2 layer, nevertheless on c-TiO_2 the solar cell did not showed other characteristics. The poor performance of the tin perovskite solar cells could be a based on oxidation effects because Sn^{4+} is much more stable than Sn^{2+}. Although the whole solar cell was prepared in the glovebox system it cannot be excluded that some oxygen and water traces were present.

2.1.1. UV-Vis spectrum

To determine the optical properties of the tin-perovskite a UV-Vis spectrum was measured. The 40 wt% tin perovskite stock solution was diluted 1:6 and coated via doctor blading on glass at room temperature to form a tin perovskite layer. All steps are performed in N_2-atmosphere.

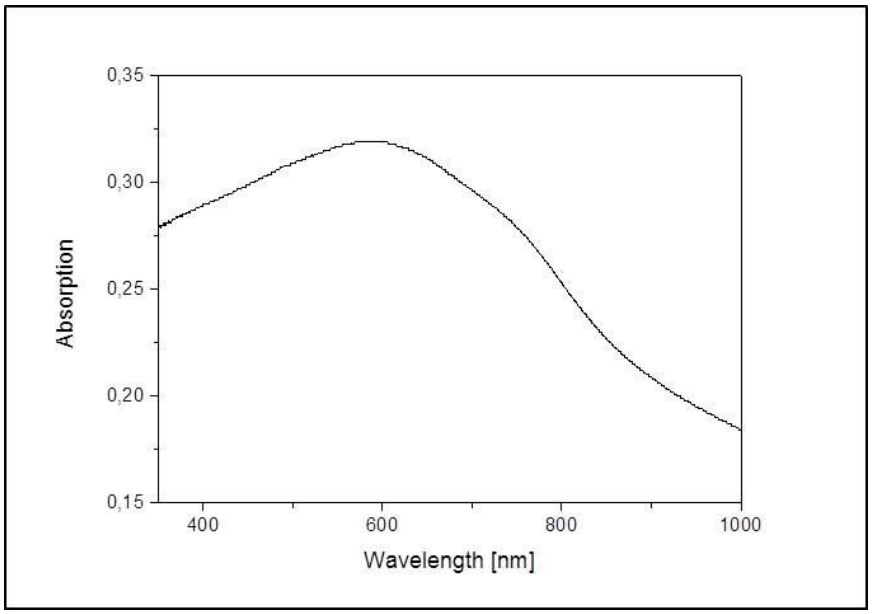

Figure 36 Absorption of tin perovskite on glass

In Figure 36 the absorption of tin perovskite on glass is shown. The absorption of tin perovskite started at a wavelength of approximately 800 nm. The tin perovskite had a broad maximum at approximately 588 nm.

2.1.2. Optical band gap determination

To see the difference in the optical band gap, transmittance and reflection measurements of tin perovskite were measured and the absorption coefficient was calculated via Equation 5 (page 58). The band gap was determined by a tauc plot. In a tauc plot $(\alpha h\nu)^2$ is plotted against the energy hν then the straight line is extrapolated to the intersection point with the x-axis.

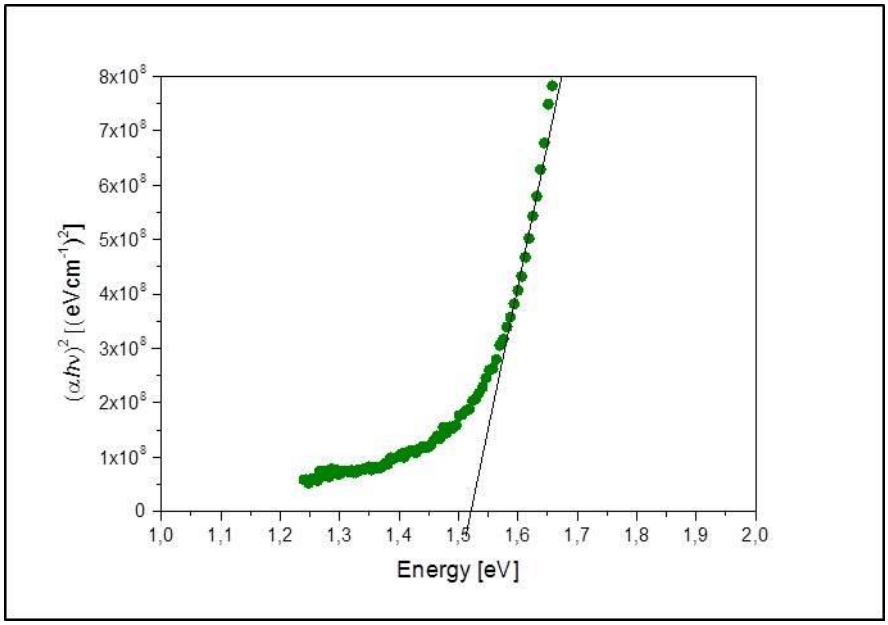

Figure 37 Band gap determination of tin perovskite

The optical band gap of the tin perovskite is 1.52 eV as it is shown in Figure 37. This is a very high value because the value in the literature are 1.3 eV[41] or 1,23 eV[27]. In the literature there is a absorption start at 900 nm reported[27], the absorption start of the tin perovskite measured was at approximately 800 nm (see Figure 36). The difference in the band gap and the shift of the absorption could be the reason why the solar cells were not working or it is an effect of the oxidation of the Sn^{2+} to Sn^{4+} in room conditions before the measurement.

2.2. BiI_3

Bismuth-triiodide (BiI_3) is a semiconductor material, which crystallizes in a perovskite similar crystal structure. BiI_3 can crystallize in a pseudo-perovskite structure. To see if there is a potential in solar cells applications, some experiments have been made.

2.2.1. Heterojunction BiI_3 solar cells

The basis for the BiI_3 solar cells was again the lead perovskite solar cell, but the fabrication conditions were adapted for the BiI_3 as active layer. Different underlayers, fabrication conditions, annealing conditions and HTMs were tested. Due to the fact that the lead solar cell worked better on a mp-TiO_x underlayer the first experiment with BiI_3 was made on mp-TiO_x. However, it looked like the BiI_3 could not penetrate into the pores of the TiO_x, so it appeared that the performance of the solar cells were the same without mp-TiO_x. The following BiI_3-solar cells were built on c-TiO_x. The heterojunction BiI_3-solar cells were coated with Spiro-OMe-TAD except it is mentioned otherwise. Due to the fact that the concentration had a very high influence on the lead solar cell the next parameter which was varied was the concentration by diluting the 40 wt% stock solution. In Figure 38 and Figure 39 the best solar cells of each device are plotted.

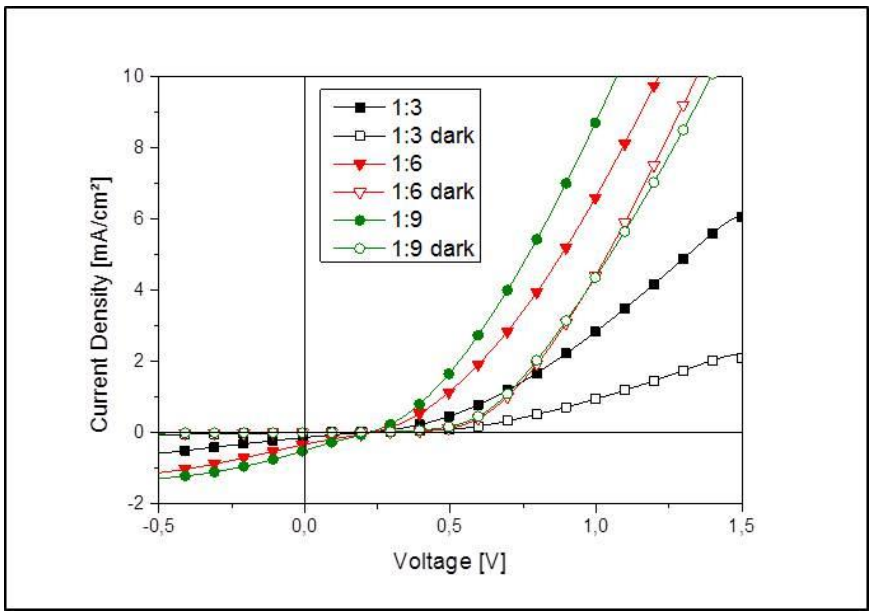

Figure 38 I-V characteristics of solar cells with different dilutions of bismuth iodide in DMSO

Glass substrate/ITO/c-TiO_x/BiI_3/Spiro + add/Au

As it is shown in Figure 38 the 1:9 dilution had the best performance with an efficiency of 0.027%. The dilutions 1:6 and 1:9 had the same V_{OC}, so that the better efficiency is only because of a higher I_{SC}. In the next experiments the annealing conditions were varied.

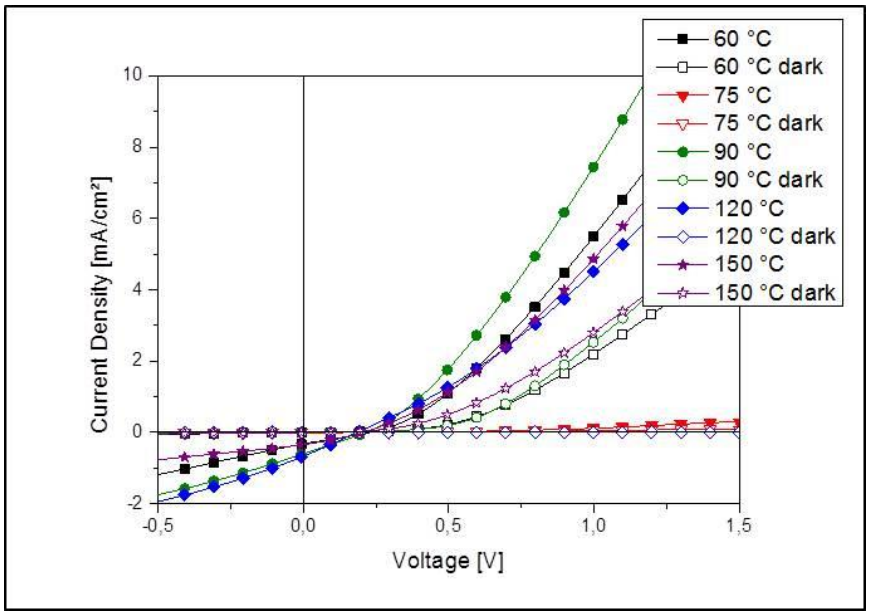

Figure 39 I-V characteristics of bismuth iodide solar cells annealed at different temperatures

Glass substrate/ITO/c-TiO_x/BiI_3/Spiro + add/Au

In Figure 39 bismuth iodide solar cells which were annealed at different temperatures are shown. The best performance had the solar cells annealed at 120 °C with an efficiency average over the best five cells of 0.028% closely followed from the device annealed at 90 °C with an efficiency average over the best five cells from 0.020%. The solar cells shown in Figure 39 with

an annealing temperature of 90 °C and 120 °C had the same efficiency of 0.032%. The variation of the annealing time had no influence on the performance of the solar cells. So that all further experiments were carried out with annealing at 120 °C or 90 °C for 40 min. Because the performances of the solar cells with a dilution of 1:6 and 1:9 and the solar cells with an annealing temperature of 90 °C and 120 °C were very similar, it was tried to reproduce the results, which are shown in Table 5.

Table 5 Solar cell parameter of the best dilutions and annealing temperatures

Glass substrate/ITO/c-TiO_x/BiI_3/Spiro + add/Au

Dilution and annealing temp.	Eff [%]	FF [%]	I_{SC} [mA/cm^2]	V_{OC} [V]
1:6 at 90 °C	0.006 ± 0.00	23.2 ± 0.54	0.131 ± 0.06	0.204 ± 0.02
1:6 at 120 °C	0.013 ± 0.00	24.9 ± 0.50	0.250 ± 0.03	0.216 ± 0.01
1:9 at 90 °C	0.016 ± 0.00	26.6 ± 1.00	0.293 ± 0.04	0.201 ± 0.00
1:9 at 120 °C	0.022 ± 0.00	26.4 ± 0.86	0.369 ± 0.04	0.224 ± 0.01
Reference cell without active layer	0.002 ± 0.00	-	0.620 ± 0.14	0.003 ± 0.00

The experiment shown in Table 5 indicated that the best fabrication parameters are a dilution of 1:9 and an annealing temperature of 120 °C. This solar cell had the highest values in all parameter except of the fill factor which was slightly higher at an annealing temperature of 90 °C and a dilution of 1:9. The reference cell shown in Table 5 is made without an active layer, the cell consists of c-TiO_x underlayer with Spiro-OMe-TAD on it. The results of the reference cell indicated that the BiI_3 active layer can convert photons into current because the efficiency of the BiI_3 solar cells is higher than the efficiency of the reference cell.

To investigate if the reason for low performance of the solar cell was the HTM, solar cells with P3HT instead of Spiro-OMe-TAD as HTM were prepared. The P3HT was coated in three different layer thicknesses but the solar cell with Spiro-OMe-TAD had the best performance.

2.2.2. BiI_3/PCBM Planar-Heterojunction Solar Cells

The perovskite/PCBM solar cells are based on a ITO-substrate coated with PEDOT:PSS. The active layer consists of BiI_3 dissolved in DMF or DMSO. The 40 wt% stock solution was diluted 1:9 and coated via doctor blading onto the PEDOT:PSS layer. The substrates were annealed for 40 min at 120 °C. Then the PCBM was coated via doctor blading on the active layer and an aluminium electrode was evaporated on top.

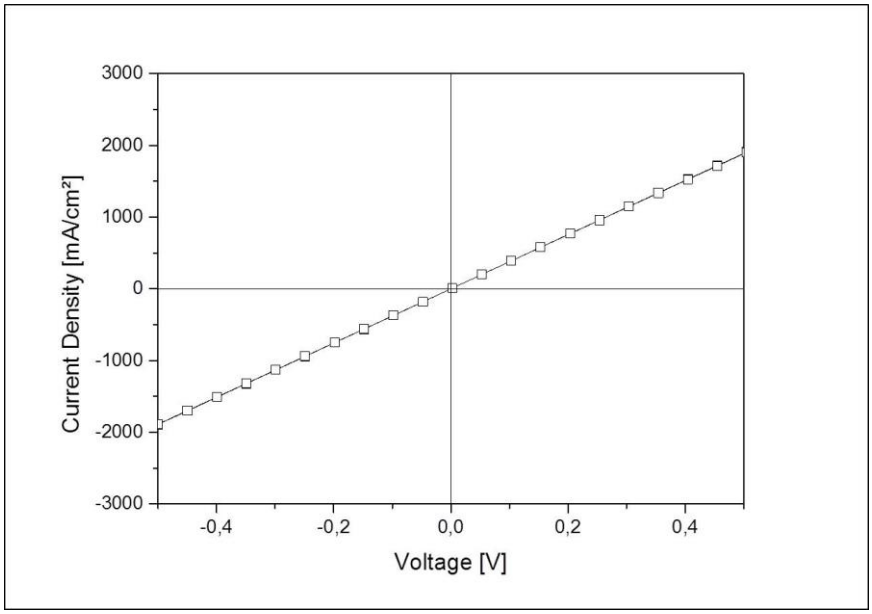

Figure 40 I-V characteristics of a BiI_3/PCBM planar heterojunction solar cell

The "solar cells" only showed a ohmic resistance, in Figure 40 one solar cell in this assembling is shown. The "solar cells" had no diode characteristics and the fill factor was not measurable, so the efficiency lacks importance. Maybe the calculated efficiency is only a measurement artefact.

2.2.3. XRD measurements

A XRD measurement was performed to see if the structure of the BiI_3 corresponds to the literature data[45].

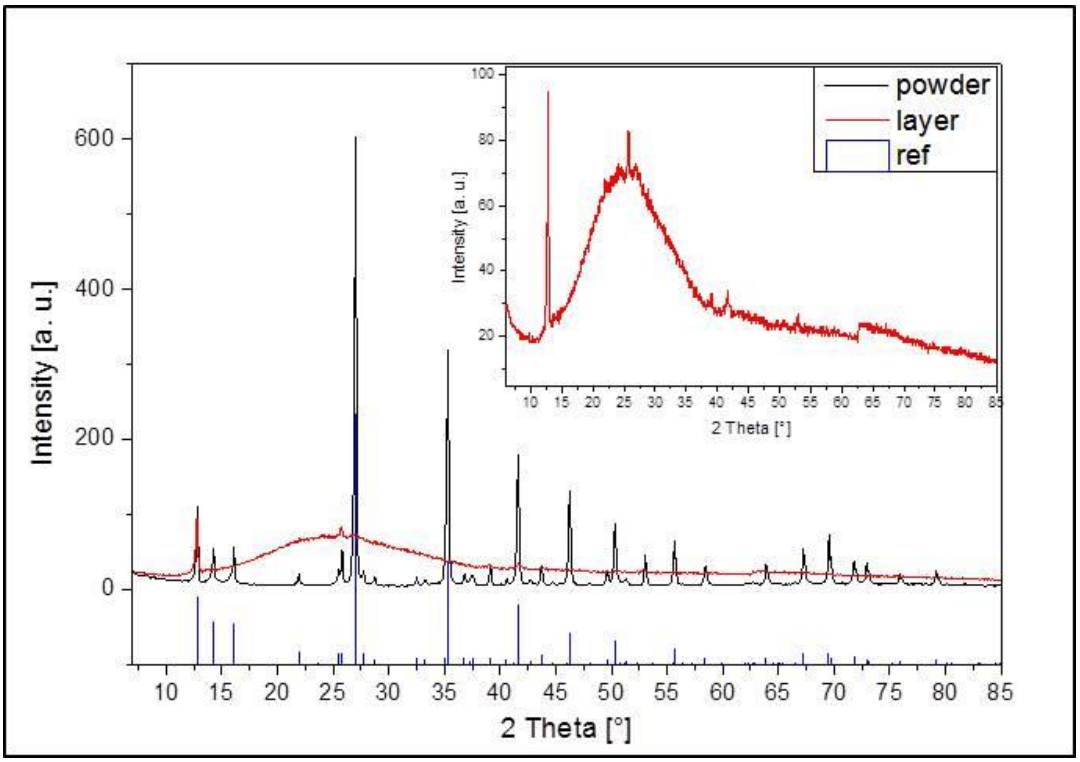

Figure 41 XRD profile of BiI_3 powder and layer und a BiI_3 reference (measured by Birgit Kunert)

In Figure 41 the diffraction pattern of BiI_3 powder and layer are shown. The small diffractogram in the diffractorgram is only zoomed depiction of the same pattern, so that the small reflection of the layer can be seen. In Figure 41 it is shown that the diffraction pattern (main signals: 12.808 ° (0 0 3), 14.251 ° (1 0 1), 26.99 ° (1 1 3), 35.27 ° (1 1 6) and 41.59 ° (3 0 0)) of the BiI_3-powder suits very well to the underneath shown reference data (Powder Diffraction File (PDF) 74-0457). According to the XRD the powder is very pure. BiI_3 has at room temperature a rhombohedral R-3 crystal structure[45,46], shown in Figure 42. In all XRD pattern no impurities signals were visible.

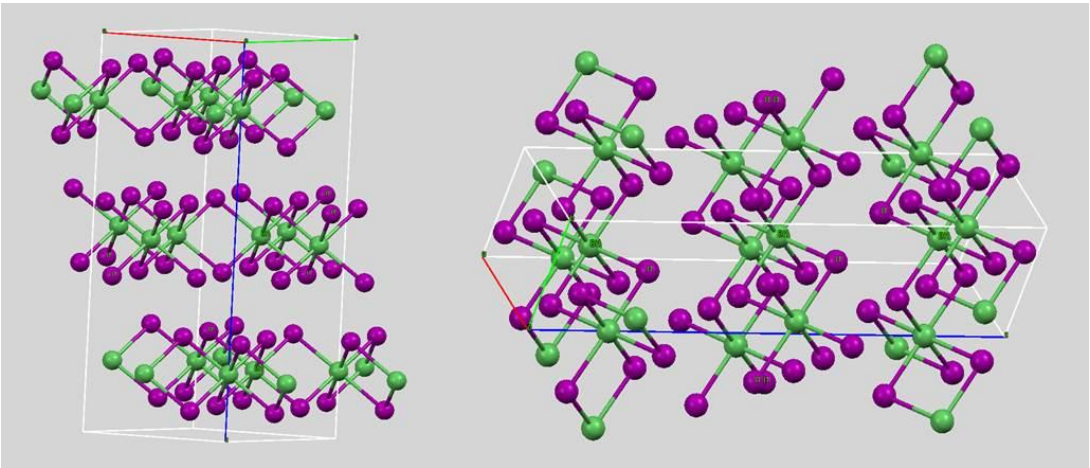

Figure 42 BiI_3 structure

The XRD pattern of the BiI_3-layer showed the characteristic glass hump. The signals (12.808 ° (0 0 3), 25.78 ° (0 0 6), 41.59 ° (3 0 0), and 52.996 (0 0 12)) belongs to BiI_3. In comparison to the XRD pattern of the powder not all lattice planes are visible. The visible lattice planes are these ones, which are parallel to the surface. In a thin layer there are some preferred orientations. The preferred orientation of the BiI_3 within the layer is shown in Figure 43 when the bottom side of the unit cell is the substrate. So the 2 D structure could be a reason why there is a very low performance of the BiI_3 solar cells.

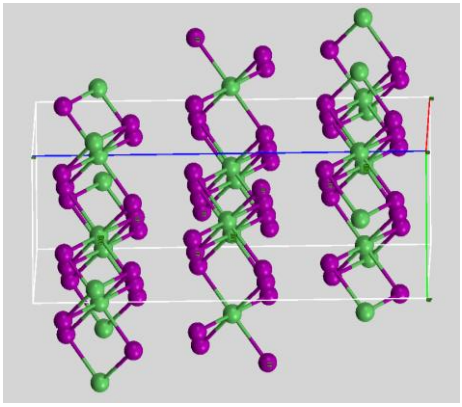

Figure 43 BiI_3 layer orientations

2.2.4. UV-Vis spectrum

To determine the optical properties of BiI_3 a UV-Vis spectrum was measured. The 40 wt% bismuth iodide pre-solution was diluted 1:9 and coated via doctor blading on glass at 60 °C. The bismuth iodide was annealed at 90 °C for 40 min. All steps are performed in N_2-atmosphere.

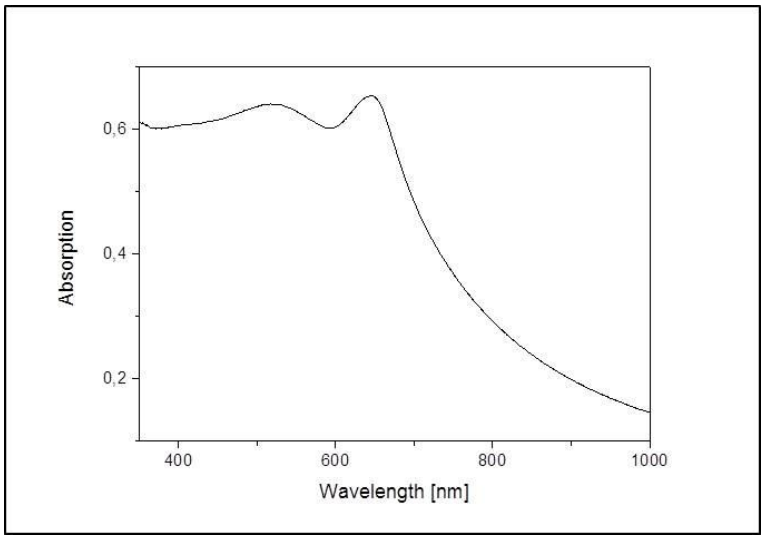

Figure 44 Absorption BiI_3 on glass

In Figure 44 the absorption of BiI_3 active layer is shown. The absorption of the BiI_3 starts at a wavelength of approximately 700 nm. The BiI_3 had a maximum at 644 nm and a second peak occurred at 517 nm.

2.2.5. Optical Band gap determination

To examine the optical band gap, transmittance and reflection measurements of BiI_3 were measured and the absorption coefficient were calculated via Equation 5 (page 58) and the band gap was determined by a tauc plot.

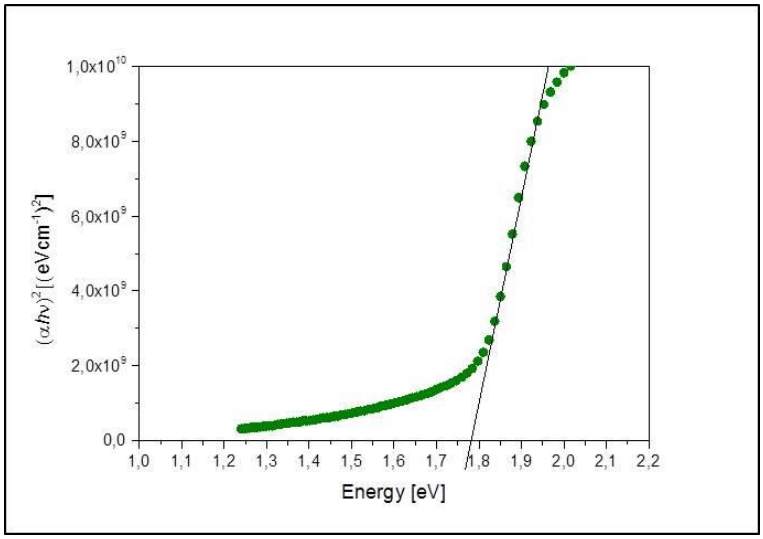

Figure 45 Band gap determination of bismuth triiodide

The optical band gap of the BiI_3 is 1.78 eV as it can be seen in Figure 45. This value suits very well to band gap of 1.67 ± 0.09 eV which is reported in the literature[45]. The absorption of BiI_3 starts at approximately 700 nm as it is shown in Figure 44.

2.3. Conclusion

Many experiments with tin perovskite in solar cells were made, but no working solar cells could be achieved. Some of them were short circuit and some had not any current flow, although different HTM and underlayers was tested. Also different way of treating the active layer brought no breakthrough.

The diode characteristics of the BiI_3 solar cells was a promising sign, but there was again a low current flow and a low voltage. Also different HTMs, different HTM layer thicknesses and a mesoporous scaffold did not improve the performance. Furthermore, no improvements could be achieved by the variation of the annealing conditions or the variation of the dilution. The other assembling with PCBM had an ever worse performance. The reason for bad performance of all built BiI_3 solar cells could be the 2D structure of the BiI_3 which was found in the XRD measurements.

IV EXPERIMENTAL

1. Materials and Equipment

In Table 6 are listed all chemicals and solvent used. All chemicals were used as received.

Table 6 Chemicals and solvents

Substance	Purity grade, solvent and description	supplier
Methylamine	40% solution in methanol	ABCR
Lead(II)iodide	99%	Sigma Aldrich
Lead(II)chloride	99,999%	Sigma Aldrich
Lead(II)thiocyanate	99,5%	Sigma Aldrich
Hydroiodic acid	55 - 58% in water	Fluka
P3HT	Sepiolid P200	Rieke Metals
Spiro-OMe-TAD	99%	1-material
Bismuth(III)iodide	99,999%	Sigma Aldrich
Tin(II)iodide	99%	ABCR
Lithium-bis-(trifluoromehtanesulfonimide)	99%	Acros organics
Bis-(trifluoromehtanesulfonyl-imide)	99%	Acros organics
[60] PCBM	99,5%	Solenne b.v.
Titanium(IV)chloride	98%	Fluka
N,N-Dimethylformamide	99,8% anhydrous	Sigma Aldrich
N-N-Dimethylformamide	99,8%	Merk
Dimethylsulfoxide	99,5%	Sigma Aldrich
2-Propanol	99,9%	Sigma Aldrich
Diethylether	99,5%	Carl Roth
Ethanol	99,5%	J.T.Baker
γ-Butyrolacton	98%	Fluka
Titanium diisopropoxide bis(acetylacetonate)	75 wt% in isopropanol	Sigma Aldrich
4-tert-Butylpyridin	96%	Sigma Aldrich

Following equipment was used for this thesis:

- X-ray Diffractometer: Siemens D501
- Doctor blade: Ericksen Coatmaster 509 MC
- Glovebox System: MBraun Labmaster DP with mounted evaporation cahmber
- Heating plate: Heidolph MR Hei-Standard
- Programmable heating plate: CAT MSC 66
- IPCE Measurement System: AMKO Xe-Lamp; Multimode 4-AT Grating Monochromator
- Photodiode for IPCE Calibration: Hamatsu Photonics S1226-18BQ
- Plasma cleaning system: Diener electronics Femto
- Profilometer: Bruker Dektak XT
- Rate/Thickness Monitor for evaporation chamber: Inficon SQM 160
- Rotovapor: Heidolph Laborota 4001
- Scanning electron microscope: Zeiss Ultra 55
- Daylight lamp for I/V measurements: Dedolight 400 D
- Source Measure Unit: Keithley 2400
- Spin coater: Karl Suss Technique S.A. CT62
- Spin coater: SPI supplies KW-4
- Ultrasonic bath: VWR Ultrasonic Cleaner
- UV/VIS Spectrometer PerkinElmer Lambda 35
- UV/VIS Spectrometer Shimadzu UV 1800

2. Preparation of Methylammoniumiodide (CH_3NH_3I)

CH_3NH_3I was synthesised by the reaction of 28 mL CH_3NH_3 40% in methanol and 30 mL of HI 55-58% in water. The CH_3NH_3 was put in a round-bottom flask under vigorous stirring and cooled with an ice bath. Then the HI was added dropwise because this reaction is exothermic. After a reaction time of two hours CH_3NH_3I was collected by evaporating the solvent in a rotary evaporator at 50 °C for 2h and washed tree-times with diethyl ether[29]. The yellowish powder was recrystallized in a mixture of diethyl ether and ethanol. The white powder was filtered and dried in vacuum for 2 hours. [47]

3. Solar cell fabrication

3.1. Cleaning of the substrates

The etched ITO substrates (Kintec, with a sheet resistance of 10 Ω /square) were cleaned with acetone followed by an ultrasonic treatment in 2-propanol (VWR ultrasonic cleaner) for 30 minutes at 50 °C. The substrates were stored in 2-propanol. Before further use the devices were cleaned in a N_2-flow to remove the dust. Then the conductive side was identified with a multimeter and put with the conductive side up in a petri dish. The ITO substrates were etched with oxygen-plasma (Diener Electronics) for three minutes to activate the surface. The plasma etching was carried out short before the deposition of the following layer because the deactivation is very fast.

3.2. Heterojunction perovskite solar cells architechture

3.2.1. Underlayer

3.2.1.1. Compact Titaniumoxide

A compact TiO_x layer was fabricated by doctor blading a 0.1 M titaniumdiisopropoxidbis-(acetylacetonate) on the substrate under ambient conditions. The speed of the doctor blading was 25 mm/s and the doctor blading process was performed at 40 °C. The precursor solution was removed by acetone from the contacting areas of the ITO electrode. After the coating the substrates were annealed for 30 min on a hotplate (Schott SLK-1) at maximum power under air to convert the precursor into titaniumoxide.

3.2.1.2. Mesoporous Titaniumoxide

When a mesoporous titaniumoxide was coated onto the compact TiO_x, the c-TiO_x substrates were treated with an aqueous-solution of titaniumtetrachloride (0.04 M) for 30 min at 70 °C under gentle stirring. After that they were rinsed with deionized water dried under a N_2-flow and annealed on a

hotplate (Schott SLK-1) at maximum power under air. For the preparation of the mesoporous titaniumoxide composed of 30-nm-sized particles a TiO_x Paste (Dyesol DSL 30NRD) was diluted in ethanol (1:3.5 weight ratio). For some mp-TiO_x layers the pre-diluted TiO_x-paste was again diluted (1:1 volume ratio) in ethanol and then deposited on the substrates by doctor blading at 40 °C with a speed of 10 mm/s. The mesoporous titaniumoxide was formed during backing in a tube furnace at 500 °C for 15 min.

3.2.2. Active layer

The active perovskite or BiI_3 layers were produced in two different ways. The first way was the solution method where an equimolare 40 wt% solution of metal dihalogenide and CH_3NH_3I in a high-boiling solvent was made, coated onto the substrate, and annealed. The second way was the dipping method. In this method a solution of metal dihalogenide in a high-boiling solvent was made, coated onto the substrate, annealed, dipped into a solution of CH_3NH_3I in 2-propanol and backed again. The annealing was always performed under inert conditions.

3.2.3. Hole transport material

As hole transport material spiro-OMe-TAD and P3HT was used. Both materials were dissolved in chlorobenzene (CB). Lithium-bis(trifluoromehtanesulfonimide) (Li-tFSI) or bis(trifluoromethane-sulfonimide) (H-tFSI) and *tert*-butylpyridin (tBP) was added to the solutions. Both solutions were coated via doctor blading at 40 °C.

3.2.4. Top electrode

The top electrode was deposited on the substrates via an evaporation step. The vacuum in the evaporation chamber in the glovebox was at least $1 * 10^{-5}$ mbar. The evaporation was carried out with MED020 from Baltec through a shadow mask to get define device area. The thickness and evaporation rate was monitored with an oscillating quartz sensor from Inficon SQM 160. As top electrode silver or gold was used.

3.3. Perovskite/PCBM Planar-Heterojunction solar cells architecture

3.3.1. Underlayer

As underlayer in this assembling PEDOT:PSS was used. The PEDOT:PSS solution (Heraeus Clevios P VP.Al 4083) was spin coated with a Karl Suss CT62 spincoater. The spincoater was accelerated with 300 rpm/s to a rotation speed of 2500 rpm and hold for 30 s. The substrate with PEDOT:PSS on it was transferred into the glovebox and dried at 150 °C for 15 min.

3.3.2. Active layer

For the active layer a mixture of metal dihalogenide and MAI or BiI_3 was dissolved in a high-boiling solvent (DMSO, GBL or DMF) to a concentration of 40 wt%. The active layer was prepared via spin coating or via doctor blading. The spin coating was performed at 3500 rpm for 45 s and the doctor blading was performed at 60 °C with a speed of 20 mm/s.

3.3.3. Hole blocking material

As hole blocking material PCBM was used, it was coated via doctor blading or via spin coating on the active layer. PCBM was dissolved in CB to a concentration of 20 m/mL or 15 mg/mL. The doctor blading parameters were 40 °C and 20 mm/s. The spin coating parameters were 1000 rpm and 60 s at room conditions.

3.3.4. Top electrode

The top electrode was deposited on the substrate as described for heterojunction perovskite solar cells. In contrast to the heterojunction perovskite solar cells aluminium was used.

3.4. Lead perovskite

All solar cells were prepared like described in IV Experimental section 3 Solar cell fabrication except it is mentions otherwise.

3.4.1. Heterojunction perovskite solar cells architecture

3.4.1.1. Different preparation processes

Device architecture: Glass/ITO/ c-TiO_x or c-TiO_x and mp-TiO_x (pre-diluted TiO_x-paste: ethanol 1:1 volume ratio)/$CH_3NH_3PbI_3$/Spiro-OMe-TAD + add/Au

PbI_2 and MAI were dissolved in DMSO to a stock solution and stirred overnight. The active layers were prepared with spin coating and doctor blading. The spin coating was performed with 4000 rpm for 30 s and the doctor blading was performed with a speed of 20 mm/s. For the first one the stock solution used as prepared and for the second one it was diluted 1:6. The active layer was annealed at 100 °C for 15 min. Spiro-OMe-TAD had a concentration of 72.3 mg/mL with 200 mM tBP and 32 mM LitFSI and was coated via doctor blading with a speed of 25 mm/s.

3.4.1.2. Different doctor blading conditions

Device architecture: Glass/ITO/c-TiO_x/$CH_3NH_3PbI_3$/P3HT + add/Au

PbI_2 and MAI were dissolved in DMSO to a stock solution and stirred overnight. The coating of the active layers was varied but for all the stock solution was diluted 1:6. The doctor blading was performed with a speed of 20 mm/s. Two were coated via doctor blading in ambient conditions with 80 °C or 60 °C. The others were coated via doctor blading in the glovebox with 40 °C or 60 °C. The active layer was annealed at 100 °C for 15 min. P3HT had a concentration of 15 mg/mL with 25 mM tBP and 76 mM Li-tFSI and was coated via doctor blading with a speed of 25 mm/s.

3.4.1.3. Different annealing temperature

Device architecture: Glass/ITO/ c-TiO_x or c-TiO_x and mp-TiO_x (pre-diluted TiO_x-paste: ethanol 1:1 volume ratio)/$CH_3NH_3PbI_3$/ Spiro-OMe-TAD + add / Ag (c-TiO_x) or Au (with mp-TiO_x)

PbI_2 and MAI were dissolved in DMSO to a stock solution and stirred overnight (c-TiO_x) or for 60 h (with mp-TiO_x). The active layers were prepared via doctor blading, which was performed with a speed of 20 mm/s and for all the stock solution was diluted 1:6. The active layer was annealed at 70 °C, 80 °C, 90 °C 100 °C, 110 °C or 120 °C for 15 min (c-TiO_x) or for 40 min (with mp-TiO_x). Spiro-OMe-TAD had a concentration of 72.3 mg/mL with 55 mM tBP and 26 mM Li-tFSI and was coated via doctor blading with a speed of 25 mm/s.

3.4.1.4. Different annealing time

Device architecture: Glass/ITO/c-TiO_x/$CH_3NH_3PbI_3$/Spiro-OMe-TAD + add /Au

PbI_2 and MAI were dissolved in DMSO to a stock solution and stirred overnight. The active layers were prepared via doctor blading, which was performed with a speed of 20 mm/s and for all the stock solution was diluted 1:6. The active layer was annealed at 90 °C for 15 min, 40 min, 60 min or 80 min. Spiro-OMe-TAD had a concentration of 72.3 mg/mL with 55 mM tBP and 26 mM Li-tFSI and was coated via doctor blading with a speed of 20 mm/s.

3.4.1.5. Different solvents

Device architecture: Glass/ITO/c-TiO_x/$CH_3NH_3PbI_3$/Spiro-OMe-TAD + add /Au

PbI_2 and MAI were dissolved in DMSO, GBL or DMSO:GBL 1:1 to a stock solution and stirred 60 h. The active layers were prepared via doctor blading, which was performed with a speed of 25 mm/s and for all the stock solution was diluted 1:6. The active layer was annealed at 90 °C for 40 min.

Spiro-OMe-TAD had a concentration of 72.3 mg/mL with 55 mM tBP and 26 mM Li-tFSI and was coated via doctor blading with a speed of 20 mm/s.

3.4.1.6. Different dilutions

Device architecture: Glass/ITO/c-TiO_x or c-TiO_x and mp-TiO_x (pre-diluted TiO_x-paste: ethanol 1:1 volume ratio)/$CH_3NH_3PbI_3$/Spiro-OMe-TAD + add /Au

PbI_2 and MAI were dissolved in DMSO to a stock solution and stirred 60 h. The stock solution was diluted 1:4, 1:5, 1:6 or 1:7. The active layers were prepared via doctor blading, which was performed with a speed of 20 mm/s. The active layer was annealed at 90 °C for 40 min. Spiro-OMe-TAD had a concentration of 72.3 mg/mL with 55 mM tBP and 26 mM Li-tFSI and was coated via doctor blading with a speed of 20 mm/s.

3.4.1.7. Optimized parameters for the solution method

Device architecture: Glass/ITO/c-TiO_x or c-TiO_x and mp-TiO_x (pre-diluted TiO_x-paste: ethanol 1:1 volume ratio)/$CH_3NH_3PbI_3$/Spiro-OMe-TAD + add or P3HT + add /Au

PbI_2 and MAI were dissolved in DMSO to a stock solution and stirred 60 h. The stock solution was diluted 1:6. The active layers were prepared via doctor blading, which was performed with a speed of 20 mm/s. Over same active layers toluene was coated via doctor blading after drying and then the active layer was annealed at 90 °C for 40 min. Spiro-OMe-TAD had a concentration of 72.3 mg/mL with 55 mM tBP and 26 mM Li-tFSI and was coated via doctor blading with a speed of 20 mm/s. P3HT had a concentration of 15 mg/mL with 25 mM tBP and 76 mM Li-tFSI and was coated via doctor blading with a speed of 20 mm/s.

3.4.1.8. Different $Pb(SCN)_2$:MAI ratio

Device architecture: Glass/ITO/c-TiO_x and mp-TiO_x (pre-diluted TiO_x-paste: ethanol 1:1 volume ratio)/$CH_3NH_3PbI_3$/Spiro-OMe-TAD + add or P3HT + add /Au

$Pb(SCN)_2$ and MAI were dissolved in DMSO in different ratios 1:1, 1:2, 1:3, 1:4 to a stock solution and stirred overnight. The stock solution was diluted 1:6. The active layers were prepared via doctor blading, which was performed with a speed of 20 mm/s. The active layer was annealed at 90 °C for 40 min. Spiro-OMe-TAD had a concentration of 72.3 mg/mL with 55 mM tBP and 26 mM Li-tFSI and was coated via doctor blading with a speed of 20 mm/s.

3.4.1.9. Different dilutions with dipping method

Device architecture: Glass/ITO/c-TiO_x and mp-TiO_x (pre-diluted TiO_x-paste: ethanol 1:1 volume ratio)/PbI_2/MAI/Spiro-OMe-TAD + add/Au

PbI_2 was dissolved in DMSO or DMF to a stock solution 462 mg/mL and stirred for 60 h. The stock solution was used as prepared or diluted 1:1, 1:3 or 1:6. The PbI_2-solution was prepared via doctor blading, which was performed with a speed of 20 mm/s. The PbI_2-layer was annealed at 70 °C for 30 min. The substrate were dipped into a 10 mg/mL solution of CH_3NH_3I in 2-propanol, washed with 2-propanol and annealed again at 70 °C for 30 min. Spiro-OMe-TAD had a concentration of 72.3 mg/mL with 55 mM tBP and 26 mM Li-tFSI and was coated via doctor blading with a speed of 20 mm/s.

3.4.1.10. Standard dipping method

Device architecture: Glass/ITO/c-TiO_x and mp-TiO_x (pre-diluted TiO_x-paste: ethanol 1:1 volume ratio)/PbX_2 (X=Cl, I, (SCN))/MAI/Spiro-OMe-TAD + add/Au

In this method the PbX_2 (X=Cl, I, (SCN)) was dissolved in DMSO or DMF to get a concentration of 462 mg/mL, stirred for 60 h and then diluted 1:1. The lead halogenide coated on the substrate via doctor blading at 60 °C and a speed of 20 mm/s. The lead halogenide layer was annealed at 70 °C or 90 °C for 30 min. Then the substrate were dipped into a 10 mg/mL solution of CH_3NH_3I in 2-propanol, washed with 2-propanol and annealed again at 70 °C or 90 °C for 30 min. Spiro-OMe-TAD had a concentration of 72.3 mg/mL with 55 mM tBP and 26 mM Li-tFSI and was coated via doctor blading with a speed of 20 mm/s.

3.4.2. Perovskite/PCBM Planar-Heterojunction solar cells architecture

3.4.2.1. Different solvent and dilutions

Device architecture: Glass/ITO/PEDOT:PSS/$CH_3NH_3PbI_3$/PCBM/Al

PbI_2 and MAI were dissolved in DMSO or DMF to a 40 wt% stock solution and stirred overnight. The active layer preparation was varied. The stock solution was diluted 1:1, 1:6, 1:8. Some were coated via spin coating and some via doctor blading. The doctor blading was performed with a speed of 20 mm/s. The active layer was annealed at 90 °C for 40 min, 60 min or 120 min.

3.5. Lead-free Perovskite

3.5.1. $CH_3NH_3SnI_3$

3.5.1.1. Heterojunction perovskite solar cells architecture

Device architecture: Glass/ITO/c-TiO_x or c-TiO_x and mp-TiO_x/$CH_3NH_3SnI_3$/ Spiro-OMe-TAD + add /Au

For the active layer an equimolar mixture of SnI_2 and CH_3NH_3I was dissolved in DMSO or DMF to a concentration of 40 wt% of the perovskite. The solution was stirred and held on 70 °C at least overnight. Only for the doctor balding the 40 wt% solution was diluted 1:1, 1:3, 1:5, 1:6, 1:7 and 1:8 volume ratios. The perovskite layer was prepared via doctor blading. The doctor blading was realized at room temperature, at 40°C and at 60°C under N_2-atmosphere with a speed of 10mm/s and 20mm/s. The perovskite layer was annealed at 50 °C or 90 °C for 40 min or 5 min or it was not annealed at all. Over some active layer toluene was coated via doctor blading as referenced[31] and to same active layer solution 1 8-diiodooctane was added as a morphology additive like reported for organic PVs[48]. As hole transport material was used Spiro-OMe-TAD at a concentration of 72.3 mg/mL or at concentration of 98 mg/mL. H-tFSI was added to the solution at a concentration of 16 mM or 10 mM. t-BP was added at a concentration of 55 mM or 80 mM. The HTM was coated via doctor blading with 20 mm/s.

3.5.2. BiI_3

3.5.2.1. Heterojunction BiI_3 solar cells architecture

Device architecture: Glass/ITO/c-TiO_x or c-TiO_x and mp-TiO_x (pre-diluted TiO_x-paste: ethanol 1:1 volume ratio)/BiI_3/ Spiro-OMe-TAD + add /Au

For the active layer a solution of BiI_3 in DMSO or DMF at a concentration of 40 wt% was prepared. The solution was stirred at 70 °C. Only for the doctor balding the 40 wt% solution was diluted 1:3, 1:6, and 1:9 volume ratios. The perovskite layer was prepared via doctor blading. The doctor blading was realized at 60°C under N_2-atmosphere with a speed of 20mm/s. The perovskite layer was annealed at 60 °C, 75 °C, 90 °C, 120 °C and 150 °C for 20 min, 40 min, 60 min or 80 min. Spiro-OMe-TAD had a concentration of 72.3 mg/mL with 55 mM tBP and 26 mM Li-tFSI and was coated via doctor blading with a speed of 20 mm/s.

3.5.2.2. BiI_3/PCBM Planar-Heterojunction Solar Cells

Device architecture: Glass/ITO/PEDOt:PSS/BiI_3/PCBM/Al

For the active layer BiI_3 was dissolved in DMSO or DMF to a concentration of 40 wt%. Before layer coating the solution was used as prepared or it was diluted 1:8 or 1:6. The active layer was prepared via doctor blading. The doctor blading was performed at 60 °C with a speed of 20 mm/s. The active layer was annealed at 90 °C for 40 min or 120 min.

3.6. Characterization

3.6.1. I-V characteristics determination

The I-V-characteristics were measured in a custom made box connected with a Keithley 2400 SourceMeter controlled by custom made LabView software. The light was generated by a Dedolight DLH400D lamp which provided a spectrum quite similar to AM1.5G. The measurement box contained a photo diode and a temperature sensor to measure the light intensity and the temperature. Every device was measured two times, once in the dark and one under illumination with an intensity of 100 mW/m². The I-V-characteristics was measured from 1.5 V to -0.5 V. All I-V-measurements were performed with a shadow mask with a size of 2 mm x 2 mm.

3.6.2. Layer Thickness and Roughness Determination

Layer thicknesses and roughnesses were determined with a Bruker DekTak XT surface profiler. To measure the layer thickness a scratch was made on the active layer and then the difference in height was measured.

3.6.3. UV-Vis spectra

For the UV-Vis-measurements the samples were prepared on glass substrates by doctor blading a 1:6 diluted 40 wt% stock solution of metal iodide (PbI_2, SnI_2) and MAI or BiI_3 at 60°C for lead perovskite and BiI_3 or at RT for tin perovskite. The absorption spectra were recorded by a UV-1800 Shimadzu UV spectrophotometer.

3.6.4. External Quantum Efficiency

EQE spectra were measured with a MuLTImode 4 monochromator equipped with a xenon lamp (AMKO) and a Keithley 2400 SourceMeter. The EQE measurements were carried out with solar cells made with the standard solution method and standard dipping method with Spiro-OMe-TAD as HTM. The solar cells were cut to a smaller size to suite into a custom made box with electric contacts in it. To contact the ITO-electrode the active layer was scratched and then coated with conductive silver lacquer. Then the box was sealed so that the solar cell had a nitrogen atmosphere during the whole measurement. Before the starting with the measurements of the solar cells a calibration with a photodiode has to be performed.

3.6.5. Optical band gap determination

The measurements to determinate the optical band gap, were carried out with UV/VIS Spectrometer Perkin Elmer Lambda 35. The 40 wt% DMSO stock solution of the lead perovskite, tin perovskite and bismuth iodide were diluted 1:6 for lead and tin perovskite and 1:9 for bismuth iodide. The substances were coated on glass and c-TiO_x, bismuth iodide and lead perovskite at 60 °C and tin perovskite at room temperature and some the layers were annealed. The tin perovskite was not annealed, the bismuth iodide was annealed for 40 min at 120 °C and the lead perovskite was annealed for 40 min at 90 °C. The absorption coefficient was calculated using the Beer–Lambert law (Equation 4) with a concentration of one for a solid state and the measured layer thickness.

$$E_\lambda = \ln\left(\frac{I_0}{I_1}\right) = \varepsilon'_\lambda * c * d$$

Equation 4 Beer-Lambert law with E_λ absorbance, I_0 intensity of incident radiation, I_1 intensity of the transmitted radiation, ε'_λ absorption coefficient, c concentration and d layer thickness

To get the absorbance of the layers transmittance and reflection were measured. The absorbance of the layer was calculated with the Beer-Lambert law where the intensity of incident radiation was one minus the reflection which is according to Kirchhoff's radiation law the absorption and transmittance and as intensity of the transmitted radiation the transmittance was used. With the combination of Beer-Lambert law and Kirchhoff's radiation law the absorption coefficient was calculated using in Equation 5

$$\alpha = \frac{1}{d}\ln\left(\frac{(1-R)}{T}\right)$$

Equation 5 Calculation of the absorption coefficient[49] with α absorption coefficient in cm^{-1}, d layer thickness, R reflection and T transmittance

3.6.6. XRD measurements

For X-ray diffraction (XRD) measurements the lead perovskite layer was prepared with the solution method on a glass substrate. A solution of PbI_2 and MAI (dilution 40 wt% stock solution 1:6) or BiI_3 (dilution 40 wt% stock solution 1:9) was coated via doctor blading at 60 °C with a speed of 20 mm/s and annealed for 40 min at 90 °C or 120 °C, respectively. Then the lead perovskite layer was scraped off the glass substrate. The samples were measured on a Siemens D 501 diffractometer in Bragg-Brentano geometry, operated at 40 kV and 30 mA, using Cu Kα radiation (λ = 1.54178 Å) and a graphite monochromator at a secondary side to obtain XRD profiles. The measurement were carried out at the Institute of Solid State Physics TU Graz by Birgit Kunert

3.6.7. Scanning Electron Microscopy

For the SEM cross section analysis solar cells made with solution method and dipping method were used. All measured solar cells had Spiro-OMeTAD as HTM and the first layer on the TiO_x was coated at 60 °C. The active layer of the solution method solar cell was annealed at 90 °C for 40 min and the dipping method solar cell was annealed twice at 70 °C for 30 min before and after dipping. As top electrode gold was used for all measured solar cells. Before the measurements the cells were broken through the top electrode. The SEM images were taken at Institute for Electron Microscopy and Nanoanalysis (FELMI) TU Graz by Dr. Angelika Reichmann

V CONCLUSION AND OUTLOOK

Perovskite solar cells are the new rock star in the solar cell community because their efficiency has increased rapidly from 4% to 20% in five years[19]. Nevertheless, lead iodide is used in the solar cells which is very harmful to the environment. In this work the fabrication conditions for a lead perovskite cell were investigated and then lead-free alternatives were tested. Therefore two substances were used in solar cell application, a tin perovskite ($CH_3NH_3SnI_3$) and BiI_3.

The first step was to try to reproduce the achievements reported in the literature[25,50]. To keep it simple the first experiment were with c-TiO_x without a mesoscopic scaffold. So the solar cell consists of an etched ITO glass substrate with a compact TiO_x layer on it then the active layer was coated on it with a solution of PbI_2 and MAI. On top of the active layer a HTM was coated and a top electrode was evaporated through a shadow mask. In the first attempts the active layer was too thick and very rough because of the big crystals in the layer. One reason for this could be that the solution of the perovskite was too concentrated or that another possibility is that the ambient conditions during the spin coating process increased the roughness. To get a smoother more homogenous layer different concentration of the precursor solutions were investigated. Furthermore the kind of coating was changed from spin coating under ambient conditions to doctor blading in a glovebox system. A lot of experiments were realized, varying the temperature during doctor blading and the annealing temperature and time in order to find the optimal crystal growth conditions. With the optimized parameters and P3HT as HTM a power conversion efficiency of 6.2% could be realized. Nevertheless it was not possible to reproduce this promising result, which again verified the assumption that the active layer formation is a very critical step in the solar cell fabrication.

Thus, further experiments were performed and it was found out, that a decreased annealing temperature (90 °C) in combination with an increased annealing time (40 min) led to an improvement in device performance. It was also recognized that with gold instead of silver as the top electrode the efficiency increased. The solvent of the perovskite could also affect the layer formation and consequently also the performance of the solar cell. As described in the literature[31] some high-boiling solvents and a mixture of them were used. The solar cell with the best performance was dissolved in DMSO and had an efficiency of 3.1%. In this solar cell Spiro-OMe-TAD was used as HTM and the solution was diluted 1:6. Moreover the dilution of the stock solution which had a concentration of 40 wt% is also an important factor. Different dilutions were tested, but the best dilution was the one with 1:6.

To further improve the performance of the solar cell a mesoscopic scaffold was used. To achieve this, the substrates with c-TiO_x were treated with $TiCl_4$ and then a diluted TiO_2 paste was coated via doctor

blading on it. The substrate was annealed twice one time before and one time after the TiO_2 paste. With the mp-TiO_x concentration of the precursor solution and annealing condition were again tested, but the best conditions were again 1:6 at 90 °C for 40 min. The direct comparison of a solar cell with and without a mp-TiO_x showed that the one with a mp-TiO_x had a better fill factor and also a better V_{OC} and I_{SC}. To see which HTM achieves a better performance solar cells with P3HT and Spiro-OMe-TAD as HTM were prepared. It showed that the solar cell with Spiro-OMe-TAD had nearly a V_{OC} twice as high as the solar cell with P3HT. The reason for this could be that there are pinholes within the P3HT layer which affect the losses of voltage. It was recognized that the time of stirring the solution has also an effect on the solar cells. For the best performing solar cells the solution was stirred for at least 72 h but not longer than 120 h. It seems that the formation of the perovskite takes some time. Another ageing effect occurred after the completion of the solar cell. This may be an ageing effect of the crystal layer or the improvement is based on the light soaking effect.

Another way to form the perovskite layer on the TiO_x is the dipping method. Therefore in a first step the PbI_2 was coated on the substrates and were annealed. Then the substrates were dipped into a solution of MAI in 2-propanol and annealed again. For this method again the best dilution of the stock solution mentioned in the literature[32] had to be found, which was figured out to be 1:1 of the stock solution with 462 mg/mL. The solar cells made with the dipping method had a better efficiency, a higher V_{OC} and a higher I_{SC} (see Figure 46) than the solution method solar cells. In Figure 46 the best solar cells of each method are shown, as HTM Spiro-OMe-TAD was used. It was also tried if the solar cells work by using another type of lead halide in dipping or solution method, but the performance of these solar cells was far beneath the performance of the lead iodide perovskite solar cell.

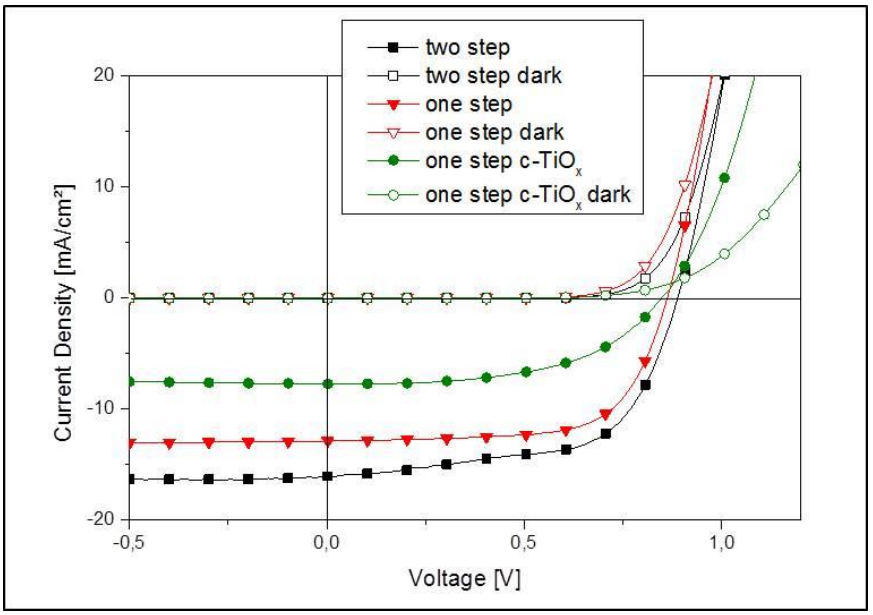

Figure 46 I-V characteristics of the best lead solar cells of each method

The lead perovskite was also used as an active layer within an organic assembling using PCBM as a hole blocking material. But all solar cells with the PCBM/perovskite assembling had a lower efficiency than the organic inorganic assembling

The best lead perovskite solar cell built was made with dipping method with 231 mg/mL PbI_2 in DMF and 10 mg/mL MAI in 2-propanol. The solar cell had a mp-TiO_x underlayer and as HTM Spiro-OMe-TAD with additives as a HTM which was coated via doctor blading at 40 °C with a speed of 20 mm/s was used. As top electrode gold was used and this solar cell had a efficiency of 8.62%.

The external quantum efficiency of the lead perovskite solar cell was up to 54% at approximately 440 nm for the solution method and approximately 50% at 450 nm for the dipping method. The measured absorption spectra fit very well to the literature[36]. The maximum of the absorption spectra were by approximately 372 nm and the maximum of the EQE measurement were by 440-450 nm. The optical band gap is 1.58 eV which matches perfect to the band gap reported in the literture[42].

The XRD measurements confirmed that the PbI_2 and the MAI crystallize in a perovskite structure, but on glass and probably also in the solar cell on c-TiO_x there remains some unreacted PbI_2 left. Maybe a mp-TiO_x underlayer could prevent this. In the SEM cross section images a difference between the solution method and the dipping method could be seen. First of all the HTM in the solution method solar cells was thicker and the active layer was thinner. In the solar cell without a mesoscopic scaffold the inhomogenous layer thicknesses of HTM and active layer could be seen, like reported in the literature[25]. This could be the reason why the solar cell on c-TiO_x had lower power conversion efficiency.

For a lead free perovskite solar cell another active layer had to be investigated. At first the lead was replaced with tin. With tin perovskite as active layer the conditions had to be adapted. So it was found that doctor blading at room temperature without annealing resulted in a smoother active layer surface and that a thicker mp-TiO_x layer showed better performance. Also different HTM were coated on the perovskite layer, but despite these efforts the solar cells with tin perovskite as active layer did not work. The best working tin perovskite solar cell was made on a mp-TiO_x with a dilution of 1:7 in DMF, coated via doctor blading with a speed of 20 mm/s at room temperature which was not annealed at all. The HTM was Spiro-OMe-TAD with additives, coated via doctor blading at 40 °C with a speed of 20 mm/s and as top electrode gold was used. The efficiency of this solar cell was $3.54 * 10^{-4}$%.

Another promising semiconductor material is BiI_3. With BiI_3 as active layer the solar cells showed a diode characteristic. For the new active layer the conditions had again to be adapted, so different dilutions and solar cell on mesoscopic and non-mesoscopic TiO_x were explored. It showed that the

kind of the TiO_x layer had no influence on the efficiency of the solar cell. The doctor blading conditions were 60 °C with a speed of 20 mm/s and the adjusted annealing conditions were 120 °C for 40 min. Nevertheless the change of the annealing time did not have an influence on the performance of the solar cell. Despite of these efforts the solar cells did not work well. Also the change of the HTM and dipping of the BiI_3-layer into a MAI solution in 2-propanol did not improve the results. The best BiI_3 solar cell was made on a c-TiO_x out of a 40 wt% solution diluted 1:9 and annealed for 40 min at 120 °C. As HTM Spiro-OMe-TAD with additives was used which was coated via doctor blading at 40 °C with a speed of 20 mm/s and as a top electrode gold was evaporated. This solar cell had an efficiency of 0.032%.

For each active layer the best solar cells all prepared via the solution method are shown in Figure 47. The 2D structure of the BiI_3 layer indicated in the XRD which could be a reason why the solar cell performance is so poor.

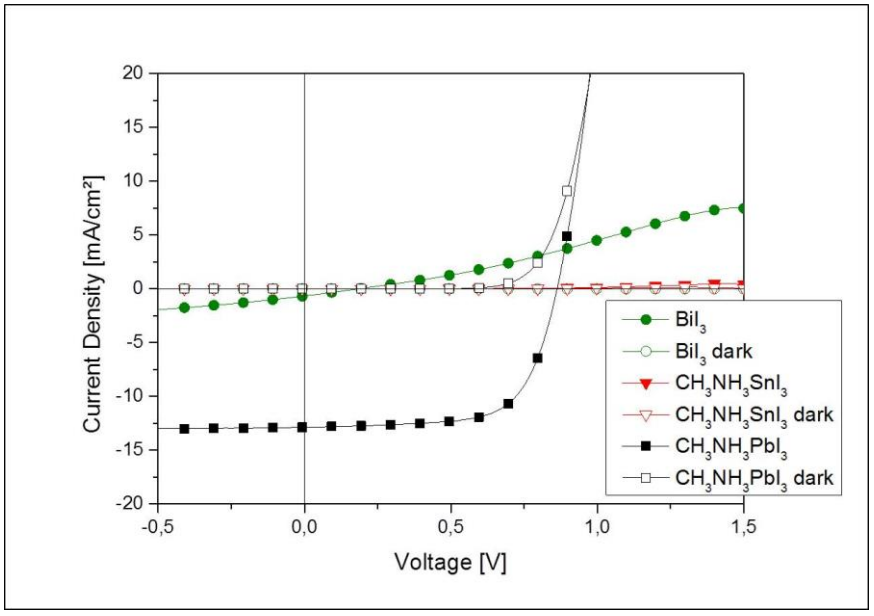

Figure 47 Best solar cells with different active layer made with solution method

In this work a good working lead solar cells was built and first experiments with lead free alternatives were performed. Nevertheless, the lead-free alternatives which were tested could not reach the performance of the lead solar cells. Maybe a deeper understanding of the crystallization of the tin perovskite could lead to higher performances. The research on BiI_3 showed that there is a potential in photoactive applications. Because of this further experiment should be made.

VI APPENDIX

5. Abbreviations

CB	Chlorobenzene
DMF	Dimethylformamid
DMSO	Dimethylsulfoxid
Eff	Efficiency
EQE	External Quantum Efficiency
FF	Fill factor
GBL	γ-Butyrolacton
I_{SC}	Short-Circuit Current
ITO	Indium Tin Oxid
I-V	Current-Volage
MCD	Material contrast detector
P3HT	Poly(3-hexylthiophene-2,5-diyl)
PCBM	Phenyl-C61-butyric acid methyl ester
PEDOT:PSS	Poly(3,4-ethylenedioxythiophene) Polystyrene sulfonate
SEM	Scanning Electron Microscopy
Spiro-MeO-TAD	2,2',7,7'-tetrakis(N,N-di-p-methoxyphenylamine)-9,9-spirobifluorene
TD	Topography detector
V_{OC}	Open circit voltage
wt%	Weight percent
XRD	X-Ray Diffraction

6. List of figures

7. List of tables

8. References

1. Nocera DG, Nash MP. Powering the planet: chemical challenges in solar energy utilization. PNAS. 2007;104(42). doi: 10.1073/pnas.0603395103.
2. Agency IE. *Key World Energy Statistics*.; 2014.
3. DRYS, P. COX G. *Official Journal of the European Union*.; 2003:6-10.
4. Cleveland CJ. Handbook of Energy. In: *Handbook of Energy*.Vol II. Elsevier; 2014:287-302. doi:10.1016/B978-0-12-417013-1.00015-7.
5. U.S. Deparment of Energy EE and RE. The Histroy of Solar Technology. *Pennyhill Press* 2013:1-12.
6. Goetzberger A, Hebling C. Photovoltaic materials, past, present, future. *Sol. Energy Mater. Sol. Cells* 2000;62(1-2):1-19. doi:10.1016/S0927-0248(99)00131-2.
7. Kim HS, Im SH, Park NG. Organolead halide perovskite: New horizons in solar cell research. *J. Phys. Chem. C* 2014;118:5615-5625. doi:10.1021/jp409025w.
8. Grätzel M. Photoelectrochemical cells. *Nature* 2001;414(November):338-344.
9. Mertens K. Aufbau und Wirkungsweise der Solarzelle. In: *Photovoltaik: Lehrbuch Zu Grundlagen, Technologie Und Praxis*.; 2013:83-112.
10. Markvart T, Castaner L. *Principles of Solar Cells Operation*. Elsevier; 2013:3-25. doi:10.1016/B978-0-12-386964-7.00001-9.
11. Chapin DM, Fuller CS, Pearson GL. A New Silicon p-n Junction Photocell for Converting Solar Radiation into Electrical Power. *J. Appl. Phys.* 1954;25(5):676. doi:10.1063/1.1721711.
12. Kong F-T, Dai S-Y, Wang K-J. Review of Recent Progress in Dye-Sensitized Solar Cells. *Adv. Optoelectron.* 2007;2007:1-13. doi:10.1155/2007/75384.
13. Chu Y. Review and Comparison of Different Solar Energy Technologies August 2011 Table of Contents. *Glob. Energy Netw. Inst.* 2011:1-52.
14. Bach U, Comte P, Moser JE, Weisso F, Gra M. Solid-state dye-sensitized mesoporous TiO2 solar cells with high photon-to-electron conversion efficiencies. *Lett. to Nat.* 1998;395(October):583-585.
15. Hulstrom CR and R. WHAT IS AN AIR MASS 1.5 SPECTRUM? *Sol. Energy Res. Inst.* 1990:1085-1088.
16. Nunzi J-M. organic photovoltaic material and devices.pdf. *C. R. Phys. 3* 2002:523–542.

17. Wright M, Uddin A. Organic—inorganic hybrid solar cells: A comparative review. *Sol. Energy Mater. Sol. Cells* 2012;107:87-111. doi:10.1016/j.solmat.2012.07.006.

18. Gao P, Gratzel M, Nazeeruddin MK. Organohalide Lead Perovskites for Photovoltaic Applications. *Energy Environ. Sci.* 2014;7:2448-2463. doi:10.1039/C4EE00942H.

19. Grätzel M. The light and shade of perovskite solar cells. *Nat. Mater.* 2014;13(9):838-842. doi:10.1038/nmat4065.

20. Lotsch B V. New light on an old story: perovskites go solar. *Angew. Chem. Int. Ed. Engl.* 2014;53(3):635-7. doi:10.1002/anie.201309368.

21. Kim H-S, Lee C-R, Im J-H, et al. Lead iodide perovskite sensitized all-solid-state submicron thin film mesoscopic solar cell with efficiency exceeding 9%. *Sci. Rep.* 2012;2:591. doi:10.1038/srep00591.

22. Snaith HJ. Perovskites: The emergence of a new era for low-cost, high-efficiency solar cells. *J. Phys. Chem. Lett.* 2013;4:3623-3630. doi:10.1021/jz4020162.

23. Lee MM, Teuscher J, Miyasaka T, Murakami TN, Snaith HJ. Efficient Hybrid Solar Cells Based on Meso-Superstructured Organometal Halide Perovskites. *Science (80-.).* 2012;338:643-647. doi:10.1126/science.1228604.

24. Snaith HJ. Perovskites: The emergence of a new era for low-cost, high-efficiency solar cells. *J. Phys. Chem. Lett.* 2013;4:3623-3630.

25. Liu M, Johnston MB, Snaith HJ. Efficient planar heterojunction perovskite solar cells by vapour deposition. *Nature* 2013;501(7467):395-8. doi:10.1038/nature12509.

26. Chen Q, Zhou H, Hong Z, et al. Planar Heterojunction Perovskite Solar Cells via Vapor-Assisted Solution Process. *J. Am. Chem. Soc.* 2014;136:622-625.

27. Noel NK, Stranks SD, Abate A, et al. Lead-Free Organic-Inorganic Tin Halide Perovskites for Photovoltaic Applications. *Energy Environ. Sci.* 2014. doi:10.1039/c4ee01076k.

28. Gonzalez-Pedro V, Juarez-Perez EJ, Arsyad WS, et al. General working principles of CH3NH3PbX3 perovskite solar cells. *Nano Lett.* 2014;14:888-893. doi:10.1021/nl404252e.

29. Lee J-W, Lee T-Y, Yoo PJ, Grätzel M, Mhaisalkar S, Park N-G. Rutile TiO2-based perovskite solar cells. *J. Mater. Chem. A* 2014;2(24):9251. doi:10.1039/c4ta01786b.

30. Wojciechowski K, Saliba M, Leijtens T, Abate A, Snaith HJ. Sub-150 °C processed meso-superstructured perovskite solar cells with enhanced efficiency. *Energy Environ. Sci.* 2014;7(3):1142. doi:10.1039/c3ee43707h.

31. Jeon NJ, Noh JH, Kim YC, Yang WS, Ryu S, Seok S Il. Solvent engineering for high-performance inorganic-organic hybrid perovskite solar cells. *Nat. Mater.* 2014;(July):1-7. doi:10.1038/nmat4014.

32. Burschka J, Pellet N, Moon S-J, et al. Sequential deposition as a route to high-performance perovskite-sensitized solar cells. *Nature* 2013;499(7458):316-9. doi:10.1038/nature12340.

33. Kim J, Kim G, Choi Y, Lee J, Heum Park S, Lee K. Light-soaking issue in polymer solar cells: Photoinduced energy level alignment at the sol-gel processed metal oxide and indium tin oxide interface. *J. Appl. Phys.* 2012;111(11):114511. doi:10.1063/1.4728173.

34. Liang P-W, Liao C-Y, Chueh C-C, et al. Additive enhanced crystallization of solution-processed perovskite for highly efficient planar-heterojunction solar cells. *Adv. Mater.* 2014;26(22):3748-54. doi:10.1002/adma.201400231.

35. Noh JH, Im SH, Heo JH, Mandal TN, Seok S Il. Chemical management for colorful, efficient, and stable inorganic-organic hybrid nanostructured solar cells. *Nano Lett.* 2013;13:1764-1769. doi:10.1021/nl400349b.

36. Liu D, Gangishetty MK, Kelly TL. Effect of CH3NH3PbI3 Thickness on Device Efficiency in Planar Heterojunction Perovskite Solar Cells. *J. Mater. Chem. A* 2014;2:19873-19881. doi:10.1039/C4TA02637C.

37. Noh JH, Im SH, Heo JH, Mandal TN, Seok S Il. Chemical Management for Colorful, Efficient, and Stable Inorganic − Organic Hybrid Nanostructured Solar Cells. *Nano Lett.* 2013;13:1764-1769. doi:10.1021/nl400349b.

38. Seok S Il. o - Methoxy Substituents in Spiro-OMeTAD for E ffi cient Inorganic − Organic Hybrid Perovskite Solar Cells. *J. Am. Chem. Soc.* 2014;136:7837-7840. doi:10.1021/ja502824c.

39. Lee D, Jang D-J. Charge-carrier relaxation dynamics of poly(3-hexylthiophene)-coated gold hybrid nanoparticles. *Polymer (Guildf).* 2014;55(21):5469-5476. doi:10.1016/j.polymer.2014.08.069.

40. Murphy a. Band-gap determination from diffuse reflectance measurements of semiconductor films, and application to photoelectrochemical water-splitting. *Sol. Energy Mater. Sol. Cells* 2007;91(14):1326-1337. doi:10.1016/j.solmat.2007.05.005.

41. Hao F, Stoumpos CC, Chang RPH, Kanatzidis MG. Anomalous band gap behavior in mixed Sn and Pb perovskites enables broadening of absorption spectrum in solar cells. *J. Am. Chem. Soc.* 2014;136(22):8094-9. doi:10.1021/ja5033259.

42. Eperon GE, Stranks SD, Menelaou C, Johnston MB, Herz LM, Snaith HJ. Formamidinium lead trihalide: a broadly tunable perovskite for efficient planar heterojunction solar cells. *Energy Environ. Sci.* 2014;7(3):982. doi:10.1039/c3ee43822h.

43. Liang PW, Liao CY, Chueh CC, et al. Additive enhanced crystallization of solution-processed perovskite for highly efficient planar-heterojunction solar cells. *Adv. Mater.* 2014;26:3748-3754. doi:10.1002/adma.201400231.

44. Hao F, Stoumpos CC, Cao DH, Chang RPH, Kanatzidis MG. Lead-free solid-state organic–inorganic halide perovskite solar cells. *Nat. Photonics* 2014;8:489-494. doi:10.1038/nphoton.2014.82.

45. Podraza NJ, Qiu W, Hinojosa BB, et al. Band gap and structure of single crystal BiI3: Resolving discrepancies in literature. *J. Appl. Phys.* 2013;114(3):033110. doi:10.1063/1.4813486.

46. Boopathi KM, Raman S, Mohanraman R, et al. Solution-processable bismuth iodide nanosheets as hole transport layers for organic solar cells. *Sol. Energy Mater. Sol. Cells* 2014;121:35-41. doi:10.1016/j.solmat.2013.10.031.

47. Etgar L, Gao P, Qin P, Graetzel M, Nazeeruddin MK. A hybrid lead iodide perovskite and lead sulfide QD heterojunction solar cell to obtain a panchromatic response. *J. Mater. Chem. A* 2014;2(30):11586. doi:10.1039/C4TA02711F.

48. Kang H, Kim K, Choi J, Lee C, Kim BJ. High-Performance All-Polymer Solar Cells Based on Face-On Stacked Polymer Blends with Low Interfacial Tension. *ACS Macro Lett.* 2014;40:1009-1014. doi:10.1021/mz500415a.

49. Khemiri N, Chaffar Akkari F, Kanzari M, Rezig B. Studies of structural and optical properties of Cu-In-O thin films. *Phys. Status Solidi* 2008;205(8):1952-1956. doi:10.1002/pssa.200778897.

50. Eperon GE, Burlakov VM, Docampo P, Goriely A, Snaith HJ. Morphological Control for High Performance, Solution-Processed Planar Heterojunction Perovskite Solar Cells. *Adv. Funct. Mater.* 2014;24(1):151-157. doi:10.1002/adfm.201302090.